Contents - E through I

NEW DUST DATA FROM STARDUST AND CASSINI MISSIONS OBTAINED BY DFMI AND HRD INSTRUMENTS. T. E. Economou, A.J. Tuzzolino, Laboratory for Astrophysics and Space Research, University of Chicago, Chicago, IL.60637.

Introduction: On January 3, 2004 the STARDUST spacecraft encounterd 81P/Wild-2 comet, performed in-situ investigation on the comet and collected cometary dust particles to bring back to Earth. On July 4, 2004 the Cassini spacecraft entered into Saturn orbit and started a multiyear study of Saturn, its satellites and its rings. The Dust Flux Monitor Instrument (DFMI) on the STARDUST mission and the High Rate Detector (HRD) on the Cassini mission, both from the University of Chicago, returned important information about the dust particle mass distribution and dust fluxes from 81P/Wild-2 comet and during multiple Saturn ring crossings.

DFMI Dust Results from 81P/Wild-2 Comet: The DFMI instrument which is based on two different technologies, has two PVDF sensors, each one with four different mass thresholds, and two acoustic counters, each one with two mass thresholds. From the data on the 12 mass thresholds, we were able to determine the cometary dust particle mass distribution in the mass regime from 10^{-14} to 10^{-6} kg [1]. The dust fux was determined throughout the flyby of the comet 81P/Wild-2 and found to be very non-uniform. The DFMI has encountered several regions of intense swarms of particles or dust clouds only a few hundred meters across. Figure 1 shows the fine time scale of dust particles distribution of one of such jet streams.

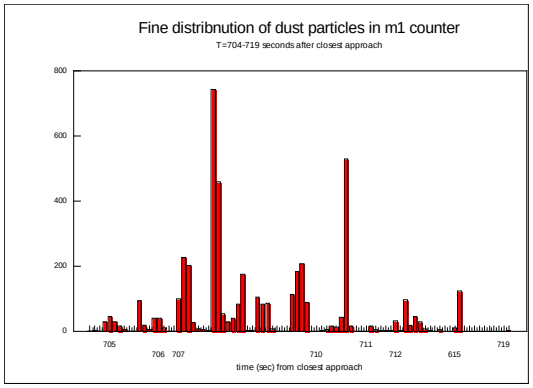

Fig. 1 showing the fine time distribution of dust particles as measured by m1 PVDF counter of the DFMI instrument during the flyby of 81P/Wild-2 comet.

The spikelike distribution of dust particle impacts was unexpected and different from previous experience. It was concluded that jets emanating from isolated emission centers on the nucleus is the primary source of the cometary activity. The characteristics of the coma structure can be easily explained by fragmentation of the fragile material coming out from the nucleus when it is subjected to several forces acting upon it [2]. Although several characteristics of the 81P/wild-2 coma differ from other comet observations and different coma models, by modifying various parameters in models, the DFMI data could be interpreted by such models [3].

HRD Dust Results from the Saturn Rings Crossings: The HRD is part of the CDA instrument on the Cassini mission and its overall objective is to obtain quantitative measurements of particle flux and mass distribution throughout the Saturn ring system, when the counting rate was expected to be very high to saturate the Dust Analyzer of the CDA instrument. The particle mass range covered by the HRD ranges from 10^{-12} to about 10^{-7} g for differential and cumulative flux measurements and $>10^{-7}$ g for cumulative flux measurements. The HRD is capable of handling counting rates up to 10^{4} impacts per second with very little dead time. The time resolution of the HRD is programmable and ranges from 1 s down to 0.1 s in the encounter mode.

Although the HRD was ON during most of the time since launch, it has seen very little activity during the entire cruise period. There are no dust data during theSaturn Orbit Insersion (SOI) because the CDA power was OFF during that period. However, the HRD has seen increase dust activity every time there was an E-ring crossing.

Especially significant activity was so far observed during the encounters with Encelladus satellite on days 2005_048 and 2005_068. Figure 2 is showing the cumulative and differential spectra during the 2005_048 crossing for M1 and m1 counters and Figure 2 is showing similar activity for the M2 and m2 counters. It is worthy to notice that the frequency of the mpacts on all counters is not uniform and shows discontinuity. From Figure 4 it can be seen that the lighter particles on m1 preceed the heavier particles on M2 at the beginning of the encounter and lag in time at the end of the encounter. That would indicate the the heavier par-

ticles are concentrated in a less space volume within the dust torus. Enceloadus seems to be one the dust particles sources for the E ring.

References:

[1] A. J. Tuzzolino, T. E. Economou, B. C. Clark, P. Tsou, D.E. Brownlee, S. F. Green, J.A.M. McDonnell, N. McBride, M. T.S.H. Colwell, Dust Measurements in the Coma of the Comet 81P/Wild 2 by the Dust Flux Monitor Instrument, SCIENCE VOL. 304 18 June 2004, pp 1776-1780.

[2] B. C. Clark, S. F. Green , T. E. Economou, S. A. Sandford, M. E. Zolensky, N. McBride, D. E. Brownlee, Release and Fragmentation of aggregates to produce heterogeneous, lumpy coma streams, J. Geoph. Res. Vol.109, E12S03, doi:10.1029/ 2004JE002319, 2004.

[3] Z. Sekanina, D. E. Brownlee, T. E. Economou, A. Tuzzolino, S. F. Green, Modeling the Nucleus and Jeets of Comet 81P/Wild 2 Based on the Stardust Encounter Data, VOL. 304 18 June 2004, pp 1769-1774.

[4] R. Srama, et al., The Cassini Cosmic Dust Analyzer, Space Science Reviews **114**, 465-518, 2004.

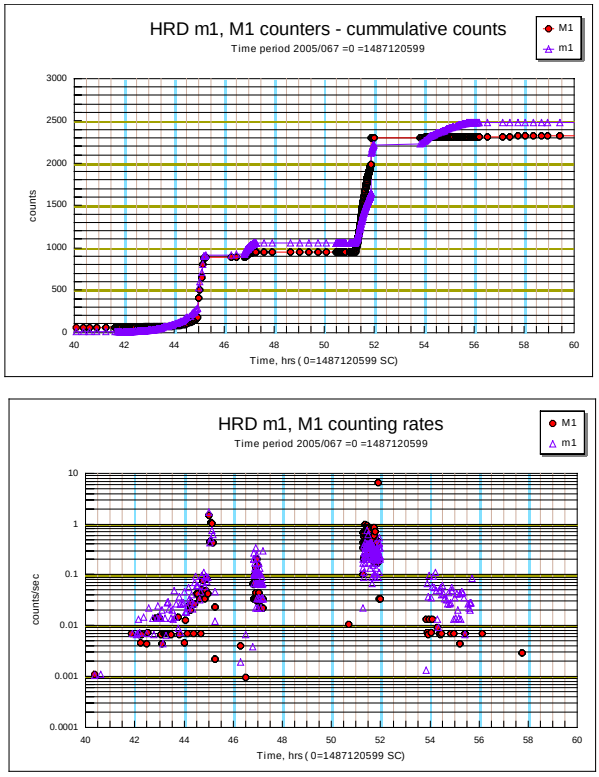

Fig.2 HRD data taken with M1 and m1 counters during Enceladus encounter on day 2005_048. On top the cumulative counts are showing, on bottom, the corresponding differential rates.

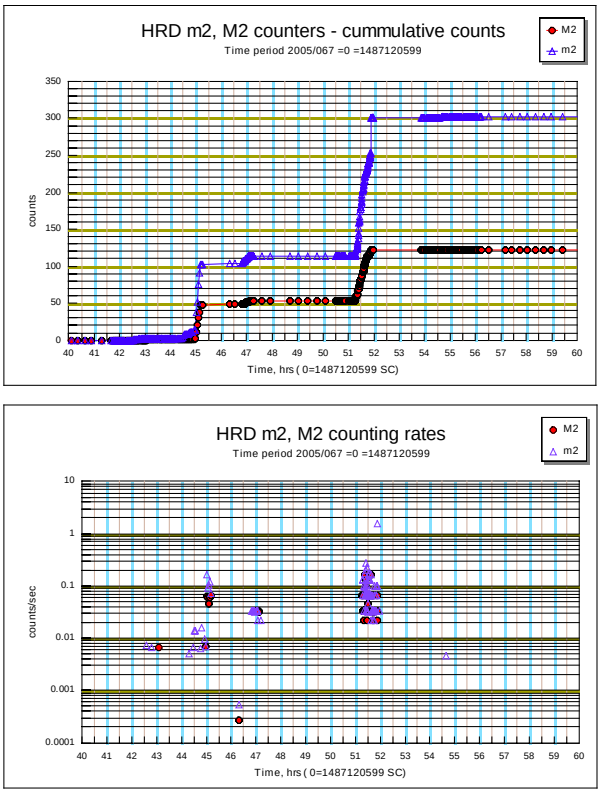

Fig.3 HRD data taken with M2 and m2 counters during Enceladus encounter on day 2005_048. On top the cumulative counts are showing, on bottom, the corresponding differential rates.

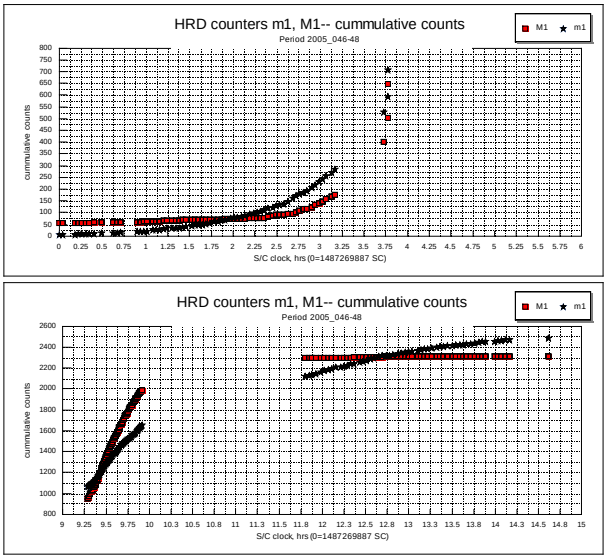

Fig.4 HRD data taken with M1 and m1 counters during Enceladus encounter on day 2005_048. On top the cumulative counts at the start of the encounter are showing, while on bottom, the corresponding cumulative counts at the end of the encounter are shown.

COMBINED MICRO-IR AND MICRO-RAMAN MEASUREMENTS ON STRATOSPHERIC IDPs. G. Ferrini[1], G. A. Baratta[2], A. Rotundi[3], M. E. Palumbo[2], L. Colangeli[1], E. Palomba[4], [1]INAF-Osservatorio Astronomico di Capodimonte, Via Moiariello, 16 - Napoli (Italy), gferrini@na.astro.it, [2]INAF-Osservatorio Astrofisico di Catania, Via Santa Sofia 78, 95123 Catania (Italy), [3]Università Parthenope, Via A. De Gasperi, 5 -Napoli (Italy), [4]INAF-Istituto di Fisica dello Spazio Interplanetario, Via del Fosso del Cavaliere 100, 00133 Roma (Italy) .

Introduction: Interplanetary Dust Particles (IDPs) provide a unique opportunity to study extraterrestrial materials in laboratory. IDPs are known to have high carbon content: 1-47 wt%, on average 2-3 times higher than that found in carbonaceous chondrites [1]. TEM studies have identified amorphous, turbostratic and poorly graphitised carbons in IDPs [2,3], other studies found organic carbons [Flynn et al, 2004, GCA. An apparent correlation between vescicular carbon and magnetite rims suggests volatiles loss during atmospheric entry flash heating [4]. The property of the carbonaceous unit in IDPs remain poorly defined [5]. Raman studies have shown that many IDPs exhibit the characteristic amorphous carbon feature. Different degrees of order could be indicative of different irradiation doses by solar wind particles and fast solar protons, suffered by IDPs in the interplanetary medium before collection in the Earth stratosphere [6].

In preparation to the STARDUST sample analyses, we performed combined micro-IR / micro-Raman measurements, supported by a FESEM investigation, on five stratospheric IDPs. We provide the IR spectral characterization of these IDPs and some new insight on the evolution of the amorphous carbon phase in IDPs The specific aim was to investigate on the potentiality of the synergry between these techniques in the identification of mineral phases other than silicates (e.g. oxides).

Experimental: Five stratospheric IDPs (L2021C13, -C20, -D9, -D12, -F17) were allocated to our laboratory by the NASA-JSC Astromaterials Curation Center (ACC). All analyses we performed on bulk grains placed on Special Sample Holders (SSHs) were non destructive [7]. We especially designed these SSHs because IDPs directly placed on them at the NASA ACC could be shipped to our laboratory where without sample manipulation the IDPs could be used for micro-IR, micro Raman and FESEM analyses

Micro-IR analyse. Micro-IR spectra have been acquired in the range 4000-600 cm^{-1} at a spectral resolution of 4 cm^{-1}, with an infrared microscope attached to a FTIR interferometer (Mod. Bruker-Equinox 55). For each particle we acquired six spectra of 6000 scans, in order to optimize the S/N ratio. The average of the six spectra was considered.

Micro-Raman analyses.. Raman microscopy was performed with a confocal microscope (by DILOR) adapted on a triplemate spectrometer (by SPEX) with a CCD detector. The objectives used gives a laser spot size on the sample of 2 µm. The laser power (Ar^+, 514.5 nm) on the sample was kept below 2 mW. No laser-induced thermal modification was detected for the IDPs studied in this work.

Results and Discussion: Micro-IR spectra of IDPs are shown in Fig. 1. The spectral classes have been assessed for IDPs -D9 and -D12 (Tab. 1). Infrared spectra of the other particles do not fall into any of the major IR spectral classes of IDPs. The results for these IDPs show the presence of oxides and sulphides in the grain mineralogy consistent with the NASA-JSC preliminary chemical EDS analyses. For particles -C13 and -F17 the IR features at about 800 cm^{-1} suggest the presence of iron oxides. The -C20 particle will require additional IR analyses to confirm the presence of iron sulphide.

L2021 -	Texture	Size (µm)	IR-class	Raman
D9	aggregate very porous	12	Ol+Py	Maghemite[1] (+Hematite[2])
D12	aggregate very porous	10x8	LLS	α-Carbon
C13	aggregate low porosity	12x10	FeO	α-Carbon (+Maghemite)
C20	spherical compact	14	FeO - FeS	Magnetite[3]
F17	cluster compact	10	FeO	Maghemite (+ Magnetite)

Table 1: IR-class* (Ol = Olivine, Py = Pyroxene, LLS = Layer Lattice Silicates) and other mineral phases (FeO = Fe-oxide-rich; FeS = Fe-sulfide-rich); Raman spectroscopy (mineral phases, (1)= γ-Fe_2O_3 [maghémite] (2)= α-Fe_2O_3, [hematite](3) = Fe_3O_4[magnetite]. *The IDP IR classification is from [8].

IDPs Raman spectra are displayed in Fig. 2. Only two of the considered IDPs (-C13, -D12) exhibit the D (Disorder) and G (graphitic) band typical of amorphous carbon (α-carbon) with intermediate degree of order. All the other IDPs exhibit the Raman

signatures typical of different forms of iron oxides (Fe_2O_3 and Fe_3O_4).

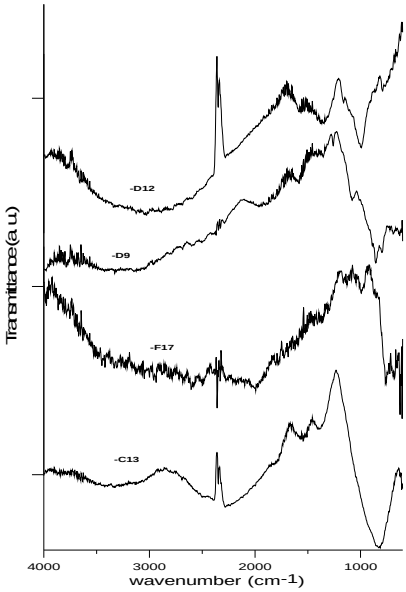

Figure 1: Micro-IR Spectra.

The Raman measurements confirm the results of micro-IR analyses and support the preliminary hypothesis on the –C20 IR characterization. The Raman bands peaking at 350, 503 and around 700 cm^{-1} typical of maghémite (γ-Fe_2O_3) [9] are present in -F17. Also the broad and poor resolved feature near 1420 cm^{-1} can be attributed to maghémite [9,10]. Maghémite signatures are visible also in the -D9 spectrum in which the additional weak bands at 224 and 292 cm^{-1} are characteristic of hematite (α-Fe_2O_3). The main bands of magnetite (Fe_3O_4) falling at 667, 545 and 305 cm^{-1} [9] are evident in the -C20 spectra. Magnetite features are also present in -F17 as indicated by its most prominent band at 667 cm^{-1}. The presence of maghémite and magnetite could indicate a severe flash heating of the particles during atmospheric entry. The formation of magnetite nanocrystals on Mg,Fe-silicate grains and magnetite or maghémite rims are due to pyrometamorphism [5, 11].

Amorphous carbon: Raman spectroscopy is a powerful tool of investigation for the study of the structure of the carbonaceous phases in IDPs [12]. Sensitive parameters are peak position, width (FWHM, Full Width at Half Maximum) and relative intensity of G and D bands. The spread in the degree of order disorder observed by Raman spectroscopy in IDPs, could be indicative of a different residence time (dose suffered) in the interplanetary medium before collection in the Earth's atmosphere [6]. The effects of

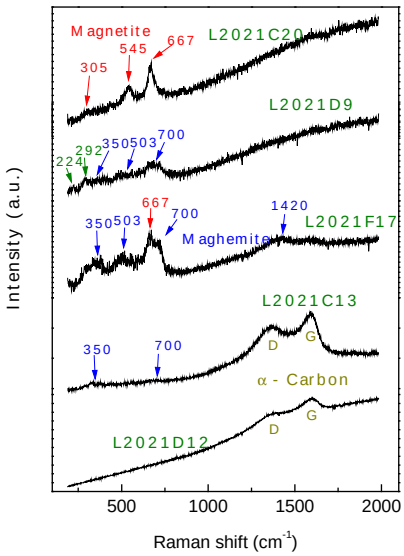

Figure 2: IDPs Raman spectra

pyrometamorphism in IDPs during atmospheric entry, can not be ruled out as a contributing factor of the measured degree of order/disorder of the carbon. Thus the indigenous structure and irradiation history of amorphous carbon in IDPs could be partially overprinted.

Conclusion: We were able to detect combination of carbon/Fe-oxides/Fe-sulfides performing combined micro-Raman and micro-IR investigations on same IDP thanks to the SSH. Same combined investigations will be applied to the Stardust grains mounted on SSHs. We will be able to detect in these particles the possible presence of the combination of Fe-oxides, Fe-sulfides and carbons that will be a diagnostic assemblage for rapid thermal heating. In particular, detecting maghémite will be strong proof of a flash-heating origin, thus it will be possible to drive conclusions on possible thermal effects due to aerogel impact.

References: [1] Keller L.P. *et al.* (1993) *AIP Conf. Proc. 310*, 159–172. [2] Rietmeijer F.J.M. and Mackinnon I.D.R. (1985) *Nature*, *315*, 733-736 .[3] Rietmeijer F.J.M. (1992) *Geochim. Cosmochim. Acta*; *56*, 1665-11671. [4] Keller L.P. et al. (1996) *LPS XXYIII*, Abstract #659. [5] Rietmeijer F.J.M. (1998) in Papike J.J., Eds., *Revs. Mineral. 36*, 2-1-2-95. [6] Baratta G.A. et al. (2004) *JRS, 35,* 487-496. [7] Palomba E. et al. (2001) *M&PS, 36,* A156. [8] Sandford, S.A. and Walker R.M (19985) ApJ, 291, 838-851. [9] Balasubramaniam R. et al. (2003) *Current Science, 11,* 1546-1555. [10] Sousa M.H. et al. (2000) *JRS, 31,* 185-191. [11] Rietmeijer (2004) *M&PS,* 39, 1869-1887. [12] Wopenka B. (1988) *E&PSL, 88,* 221–231.

CIR MODULATION OF JUPITER DUST STREAM DETECTION

A. Flandes[1] and H Krüger
[1]Instituto de Geofisica (UNAM) xytrahx@yahoo.com.mx

During late 2003 and early 2004, Ulysses approached Jupiter (~0.8 AU at its closest distance) and detected 24 new dust streams. The tiny positively charged dust grains (~10nm) in the streams are pushed away from Jupiter by its co-rotational electric field, accelerating them to very high speeds (>200 km/s). Once outside the Jovian magnetosphere, dust grains are under the influence of the interplanetary magnetic field and some characteristics of this field are observable on the streams. Dust streams seem to be correlated to the solar *Co-rotating Interacting Regions* (CIR). On the whole, there seems to be a previous CIR for every set of streams. The duration of the set of steams matches roughly the duration of the CIRs, indicating a confinement of the dust stream particles in the compressed regions of the interplanetary plasma. On the other hand, most dust stream peaks and the precedent CIR peaks seem to be separated by an interval roughly similar to the time needed by a dust particle to travel from the source to the spacecraft's detector.

ELEMENT HOSTS IN ANHYDROUS IDPS: A TEST OF NEBULA CONDENSATION MODELS.. G. J. Flynn[1], L. P. Keller[2], and S. R. Sutton[3], [1]Dept. of Physics, SUNY-Plattsburgh, Plattsburgh NY 12901, USA. george.flynn@plattsburgh.edu. [2]NASA Johnson Space Center, Houston, TX 77058. [3]Dept of Geophysical Sciences and CARS, The University of Chicago, Chicago, IL 60637.

Introduction: Many anhydrous interplanetary dust particles (IDPs) are the most pristine samples of primitive Solar System dust that are currently available for laboratory analysis. Because these primitive, anhydrous IDPs show little or no evidence that they have experienced either thermal or aqueous alteration since their formation, they preserve materials that formed in the early Solar Nebula as well as presolar materials. Thus, we can test the applicability of equilibrium nebula condensation models to our Solar System by comparing the host mineral of each element with the host that is predicted by the nebula condensation models.

Samples: We have mapped the spatial distribution of most of the elements from K to Zn in ultramicrotome sections, each ~100 nm thick, in 3 primitive, anhydrous IDPs – L2011*B2, L2010B10, and L2009*F3, all of which are fragments of cluster IDPs. We employed a zone plate focused X-Ray Microprobe (XRM) at Sector 2 of the Advanced Photon Source (APS) at the Argonne National Laboratory to perform the element mapping. This XRM has ~150 nm spatial resolution, which is sufficient to resolve individual mineral grains in most of the anhydrous IDPs.

Results: Each element was found to be localized within each IDP, with some hot-spots being sub-micron is size.

K Results. L2011*B2 is a cluster fragment that contains a relatively high K concentration. The K is spatially correlated with the silicate in this particle (see Fig. 1). Nebula condensation models indicate that K should condense at ~1000 K into K-feldspar [1, 2]. However, Transmission Electron Microscope (TEM) examination of other ultramicrotome sections of this fragment indicate that the silicate in L2011*B2 is pyroxene, rather than feldspar.

S Results, Small S hot-spots were detected in each IDP. Most of the S is concentrated in Fe-sulfides, consistent with the prediction of nebula condensation models that S should condense at ~650 K into Fe-sulfide [1, 2].

Zn Results, The Zn is concentrated into small hot spots, which are collocated with S. However, the Fe K-alpha peak is significantly higher than the Zn K-alpha peak in the spectrum of the Zn hot-spot, indicating that the Zn host is either a Zn-rich Fe-sulfide, or Fe- and Zn-sulfides are intermixed on a size scale that is small compared to the analysis spot. The nebula condensation models generally include the thermodynamic properties of only pure Zn-sulfide, and predict that Zn should condense at ~660 K into Zn-sulfide [1, 2].

Cu Results: The Cu is concentrated into hot spots, which are collocated with S. The equilibrium nebula condensation models predict Cu condenses at ~1040 K into a metal [1, 2].

Cr Results: The Cr is concentrated into hot spots (see Fig. 2), which are collocated with Si, Ca, and Fe (see Fig. 3) indicating the Cr-host is an Fe-silicate. In most nebula condensation models, Cr condenses into Fe-metal, which alters to Fe-Cr oxide (a Cr-spinel) as the nebula cools further.

Ca, Ti, Cr, Mn, and Ni Results, We also observed hot-spots of Ca, Ti, Cr, Mn, and Ni in the element maps. The host minerals of each of these elements will be determined by TEM, and compared to the predictions of the equilibrium nebula condensation models.

Conclusions: High spatial resolution chemical mapping of the most primitive IDPs provides a way to test nebula condensation models. The results of this project should provide important information on the minerals whose thermodynamic properties should be included in future models.

References: [1] Grossman, L. 1972, *Geoch. Cosmochim. Acta*, **36**, 597-619. [2] Grossman, L. and Larimer, J. W. 1974, *Reviews of Geophys. and Space Physics*, **12**, 71-101.

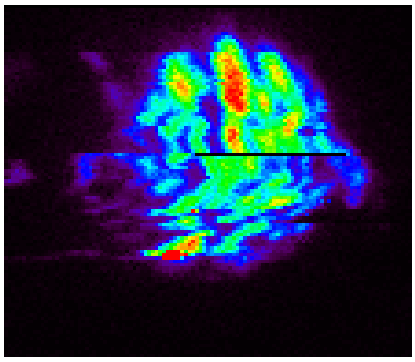

Figure 1: K map of L2011*B2. Bright areas are highest concentration. The K-rich areas are also high in Si.

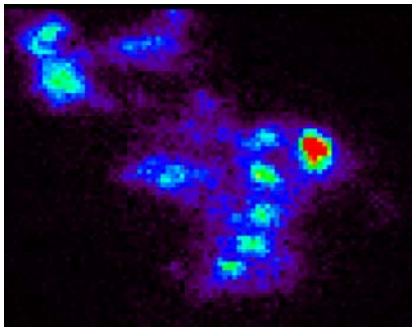

Figure 2: Cr map of L2009*F3.

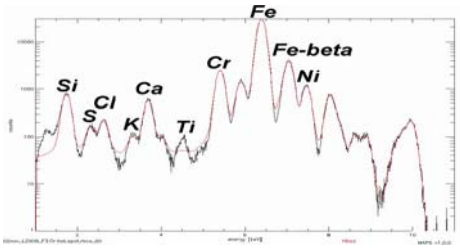

Figure 3: X-ray fluorescence spectrum of Cr hot-spot in L2009*F3.

TENTATIVE IDENTIFICATION OF INTERSTELLAR DUST TOWARDS THE HELIOSPHERE NOSE. P. C. Frisch. Department of Astronomy and Astrophysics, University of Chicago, 5640 South Ellis Ave., Chicago, Il 60637, U.S.A.

Optical polarization data from Tinbergen (1982), which show the weak polarization of light for stars within 35 pc of the Sun, are reinterpreted to show an origin consistent with the entrainment of the polarizing grains in the outer heliosheath. The original data indicated that a small patch of polarizing dust grains are present within ~35 pc of the Sun near the galactic center region. It is shown here that both the region of maximum polarization and polarization position angle suggest an origin associated with small grain entrainment in the interstellar magnetic field draped over the heliosphere. The region with best grain alignment as measured by correlated position angels, ecliptic longitude $\lambda = 281° \rightarrow 330°$, is offset by over 20° from the upwind direction. The region showing maximum polarization is centered near $\lambda = 295°$, $\beta = 0°$ (ecliptic coordinates), compared to the heliosphere nose direction $\lambda = 259°$, $\beta = +5°$. The polarization strength anticorrelates with ecliptic latitude in this region. These properties are consistent if the polarization is caused by small interstellar grains, radii <1 micron, aligned by the interstellar magnetic field draped aroudn the heliosheath. If this interpretation is correct, these trapped interstellar dust grains provide a means of monitoring the outer heliosheath over the solar cycle, and may possibly contaminate the cosmic microwave background.

HAYABUSA MISSION TO ASTEROID ITOKAWA: IN-SITU OBSERVATION AND SAMPLE RETURN.

A. Fujiwara[1], J. Kawaguchi[1], S. Sasaki[2], & Hayabusa Team, [1]ISAS/JAXA (The Institute of Space and Astronautical Science of Japan Aerospace Exploration Agency) 3-1-1 Yoshinodai, Sagamihara, 229-8510, JAPAN (fujiwara@planeta.sci.isas.ac.jp), [2] National Astronomical Observatory of Japan, 2-12 Hoshigaoka, Mizusawa, 023-0861, JAPAN (sho@miz.nao.ac.jp).

Introduction:

Recent direct observations of asteroids by spacecrafts are revealing their various interesting characteristics which cannot be obtained either from ground-based observations or meteorite studies. However, identification of the real material species constituting asteroids and their corresponding meteorite analogs are still ambiguous. Space weathering process makes it difficult to identify the real material, and there is still a great gap between the remote sensing data (from the ground and/or from spacecrafts) and the local microscopic data from meteorites. Surface of many asteroids may be covered with fine regolith materials which would be different from usual meteorite specimen. Sample return missions from asteroids are indispensable to solve these problems. HAYABUSA (MUSES-C) spacecraft which was launched on May 9th 2003 is the first attempt on the sample return from an asteroid. Here outline of the mission is described with special emphasis on its science.

Outline of mission:

HAYABUSA is an engineering spacecraft to develop technologies required for future missions such as electric propulsion, autonomous navigation, sampling, and reentry technique [1]. The spacecraft is three-axis stabilized, its dry weight is 380kg, and the total weight including chemical fuel and Xe propellant is 510kg. The target asteroid is Itokawa (1998 SF36) among Apollo group of near-earth asteroids. Properties of the target asteroid were extensively studied [2-4]. The orbital elements are a= 1.324AU, e=0.279, q=0.955AU, Q=1.693AU, and i=1.713deg. From radar observations, diameter is estimated to be approximately 600m x 300m. Rotation period is 12.1 hours and the rotational axis is supposed to be almost perpendicular to the ecliptic plane. The provisional spectral type is S and corresponding meteoritic type is considered to be LL ordinary chondrite [4].

On May 9, 2003. HAYABUSA was launched successfully by an M-V rocket from Kagoshima Space Center. It made a fly-by with the earth in May 2004 and was transferred to the orbit toward the target asteroid. by gravity assist. HAYABUSA approach Itokawa in September 2005. It hovers above the asteroid surface at the sunlit side at altitude of about 7km. From this home position, HAYABUSA will perform global mapping of the asteroid. Rotation period of Itokawa is 12.1 hours. Although HAYABUSA spends most of time near the home position, it will also approach the terminator side of the asteroid. On the basis of information obtained from remote sensing observation, sampling points are determined from the viewpoint of the safety of the spacecraft and the scientific interest. In early November 2005, HAYABUSA will descend to the asteroid surface to make sampling of the surface material. After the descent to altitude about 20m by LIDAR, HAYABUSA will deploy a target marker for the touchdown and a small robotic rover called MINERVA. The target marker is used as the artificial target to be referred for the descent. The MINERVA hops on the asteroid surface by the reaction of the two torquers installed in it. Sampling of asteroid material is carried out by shooting a small projectile onto the asteroid surface and catching the ejected material. Just after the contact of the sampling device with the asteroid surface, HAYABUSA will start rising back to the home position. Sampling will be carried out from two different locations on the asteroid surface.

The spacecraft will leave the asteroid Itokawa (hovering position) in December 2005, and after cruising under the operation of the ion engine it will approach the earth in June 2007. The reentry capsule separated from the spacecraft plunges into the earth atmosphere at velocity 12km/s directly from the interplanetary orbit. After sufficient deceleration in the earth atmosphere a parachute is deployed and the front ablator shield is removed off to avoid the additional heat invasion into the sample canister. The landing site is scheduled to be Woomera desert in Australia.

Scientific instruments:

Scientific instruments on board are a CCD imaging camera (AMICA) with 8 filters of wavelength bands similaer to the ECAS system and polarizers, a near-infrared spectrometer (NIRS), a light detection and ranging device (LIDAR) using a YAG pulse laser emitter and a Si-APD receiver, and a CCD X-ray fluorescence spectrometer (XRS) (see Table 1). Under corporation with NASA, several instruments involve co-investigators from U.S.

Primary objective of AMICA and LIDAR is for navigation, but they play important roles to obtain topographical data of the asteroid surface. Ranging data by LIDAR provides the information of the asteroid gravity and mass. Coupled with the asteroid shape data, Itokawa's density will be estimated. Spatial resolution of the asteroid surface by the AMICA is less than 10 m at the home position. Search for satellites and dust particles around Itokawa will be also conducted by AMICA. NIRS is an InGaAs 64 pixel linear array detector, and the wavelength covered is 0.85-2.10 micron. NIRS will provide valuable data on surface mineralogy of Itokawa and ongoing space weathering process. XRS has energy resolution 100eV at 1.5keV, and can detect Fe, Na, Mg, Al, Si, and S. All these instruments are installed on the base panel of the spacecraft. The MINERVA has three miniature cameras to obtain stereoscopic images and different focal lengths images of the asteroid surface and landscape. It also has six platinum thermometers and they measure the surface temperature.

The sampling device is also installed on the base panel. Its main part is the funnel-type tube called a horn of length 1m and diameter 20cm. Immediately after sensing the contact of the bottom of the horn with the asteroid surface the projectile of mass 5g made of tantalum is shot at velocity 300m/s and asteroidal fragments are ejected. The sample through passing the horn is caught by the canister attached on the top of the horn. Microgravity experiments confirmed that this shooting method can collect either rocky or regolith materials on the surface. Total amount of the sample will be expected to be about 1g [5]. The spacecraft lifts off the asteroid surface with the aid of chemical thrusters within a few second after the contact to avoid the damage by the contact of the tumbling main body with the asteroid surface. The samples from two different locations are separately enclosed in the small canister rooms and the canister is transferred into the reentry capsule mounted on the side panel of the spacecraft. The canister is sealed by double O-rings and the sample is separated from the outside environment.

Sample analysis:

The asteroid sample in the canister retrieved in Australia is transferred to a curation facility at ISAS/JAXA. After fundamental characterization some portion of the samples is separated and distributed for the initial analysis. The initial analysis will be carried out on the scheduled program in several facilities in Japan by the MASPET team consisting of Japanese, US, and Australian scientists during about one year. In the following detailed analysis phase, the samples will be distributed to the researchers all over the world on the basis of AO.

Conclusion:

HAYABUSA is the first sample return mission from an asteroid. During its rendezvous phase with the target asteroid Itokawa, HAYABUSA will provide first detailed image of topographic feature of an asteroid of diameter less than 1km, and be able to answer whether regolith exists or not on such a small body and whether the body is monolithic or not. It will also able to find mineralogical and chemical inhomogeneity with sufficient spatial resolution, if it exists. The remote sensing instruments (AMICA, NIRS, XRS) boarded on the spacecraft will provide global, but in various spatial scale, mineralogical and elemental abundance data along with the topographical data from AMICA, LIDAR, and MINERVA cameras. The returned sample will provide the detailed and abundant chemical, mineralogical, and physical information of the asteroid surface in the finest scale, which enables to make direct comparison with meteorite data. These data will be used to establish a strong link between the asteroids of S-type spectra obtained by ground-based observation and material properties obtained from meteorite research

References: [1] Kawaguchi, J et al. (2003) *Acta Astronautica, 52,* 117–123. [2] Ohba, Y. et al. (2003) *Earth Planets Spac,e55,* 341-347. [3] Ishiguro, M. et al (2003)*Publ. Astron. Soc. Japan 55,* 691–699. [4] Binzel, R. et al. (2001) *Meteorit.Olanet. Sci. 31,* 1167 [5] Yano, H. et al. (2002) *Proc. ACM 2002(ESA SP500),* 103-106.

Table 1
Instruments and sciences on HAYABUSA mission

Instrument/Theme	Team Leader	
AMICA	J. Saito	ISAS/JAXA
NIRS	M. Abe	ISAS/JAXA
LIDAR	T. Mukai	Kobe U.
XRS	M. Kato	ISAS/JAXA
MINERVA		
(Technology)	T. Yoshimitsu	ISAS/JAXA
(Science)	S. Sasaki	NAOJ
Astrodynamics	M. Yoshikawa	ISAS/JAXA
Sample Analysis	T. Yamamoto	Hokkaido U.
	(formerly I. Kushiro	JAMSTEC)
ISAS Project Manager	J. Kawaguchi	
ISAS Project Scientist	A. Fujiwara	
NASA Project Scientist	D. Yeomans	

THE PARENT BODIES OF MICROMETEORITES. M. J. Genge, Impact and Astromaterials Research Centre (IARC), Imperial College London & The Natural History Museum, Exhibition Road, London SW7 2AZ, UK. Email: m.genge@imperial.ac.uk.

Introduction: Micrometeorites (MMs) are that fraction of the Earth's extraterrestrial dust flux that survives atmospheric entry to be recovered from the Earth's surface. Large numbers of MMs have been collected from Antarctic ice [1] and provide an important sample of dust present in the Zodiacal cloud at 1 AU for direct study in the laboratory using micro-analysis.

The capture mechanics of dust by the Earth favours those interplanetary dust particles with low geocentric velocities and low ecliptic latitudes at 1 AU and thus asteroidal sources with the lowest inclinations and eccentricities are likely to make the largest contributions. Low geocentric velocity dust is also more likely to survive atmospheric entry without significant heating to be recovered at the surface of the Earth [e.g. 2,3].

The current study presents mineralogical, textural and compositional data on 730 micrometeorites recovered from Antarctic ice that allows the parent body affinities of these materials to be tested. It is argued on the basis of the distribution of particle types that MMs are derived predominately from four main genetic groups of parent body of which three have close affinities to chondritic meteorites and the fourth may be closely related to cometary materials, albeit with what are currently considered definitively asteroidal characteristics.

Samples and Methods: The MMs described in this study are 50-400 μm in size and were collected from Antarctic blue ice near Cap Prudhomme. Analytical and separation techniques are described in Genge et al., [4].

The Relative Abundances of MM Types: Micrometeorites can be split into two main groups on the basis of the degree of heating during atmospheric entry: (1) unmelted particles and (2) melted and partially melted particles. This study focuses on unmelted particles that preserve sufficient mineralogical and textural features to allow their parent body affinities to be assessed. This approach, however, introduces a bias towards those particles comprised principally of high temperature components.

Unmelted MMs include two main particle types: (1) fine-grained MMs (fgMMs), with sub-micron grain-sizes, and textural and compositional affinities to the hydrated matrices of carbonaceous chondrites and (2) coarse-grained MMs (cgMMs), which are dominated by pyroxene, olivine and glass, and usually have igneous textures.

Fine-grained MMs can be sub-divided into three gradational classes on the basis of texture and mineralogy. (a) C1 particles consist of low porosity matrix comprised of phyllosilicates (clay minerals) or their dehydration products with few anhydrous silicates. The matrices of C1 particles show little spatial variation in Fe-content over scales of 10-100 μm similar to CI1 chondrites [5] and implies extensive elemental mobility during aqueous alteration and high water to rock ratios. (b) C2 particles are dominated by low porosity matrix consisting of phyllosilicates (or their thermal decomposition products). The matrices of C2 particles show up to 10 wt% variation in Fe content over 10-100 μm and include much higher abundances of anhydrous silicates including Fe-rich pyroxenes, which are sensitive to aqueous alteration. The mineralogies and textures of C2 particles are broadly similar to those of CM2 chondrites [5] and suggest limited elemental mobility and lower water to rock ratios than C1 particles. (c) C3 particles consist of high porosity matrices (up to 50% by volume) dominated by micron-sized olivine and pyroxene grains. These are, however, a diverse group of particles and many contain variable amounts of interstitial phyllosilicate (or dehydration product). The matrices of C3 particles show little variatiation in Fe content over 10-100 μm scales and contain relatively abundant isolated (>4 μm) pyroxene and olivines grains. The presence of phyllosilicate and framboidal magnetite within C3 particles suggests they have experienced a degree of aqueous alteration, however, their high porosities indicate this was less than C1 or C2 particles. C3 particles have no direct meteorite equivalents.

Coarse-grained MMs are a group of particles dominated by pyroxene, olivine and glass that have broadly similar mineralogies, compostions and textures to chondrules found within chondritic meteorites. The principal evidence that cgMMs represent fragments of chondrules is: (1) the majority of cgMMs fall into either reduced, oxidized or radiating pyroxene groups similar to chondrules, (2) the grain-sizes of cgMMs is <50 μm and not consistent with most achondritic (igneous differentiated meteorites), and (3) cgMMs often have unequilibrated mineral assemblages indicating non-equilibrium crystallization. To date only a single

cgMM has been identified that is demonstrably achondritic [6].

Composite MMs consisting of fine-grained and coarse-grained portions are highly significant since these indicate that cgMMs sample small igneous objects which were embedded in C2 fine-grained matrix [7]. These composite MMs are dominated (>70%) by reduced igneous objects suggesting a close affinity to CM2 chondrites that are dominated by reduced (Type I) chondrules. The overall abundance of composite MMs (which sample the chondrule/matrix interface) to cgMMs (which are interior fragments of chondrules) suggests an average chondrule diameter of ~1600 μm larger than in any meteorite group [8].

The abundance of cgMM also suggests differences from CM2 chondrites. Chondrules comprise ~15% by volume of CM2's and yet the abundance of cgMMs is approximately equal to that of fgMMs. Furthermore CM2 chondrules are dominated by Type I (reduced chondrules) [5] and yet ~40% of cgMMs are oxidized (Type II) materials. These data suggest that a significant proportion of cgMMs are derived from a chondrule-dominated source containing abundant Type II chondrules. This source would, therefore, have affinities to ordinary chondrites [5]. Chromium and Mn contents of olivines from some cgMM support this hypothesis since they fall in the range of those of ordinary chondrites. The occurrence of glass in the majority of cgMMs furthermore indicates an unequilibrated source.

Although cgMMs usually preserve glass indicating no significant metamorphism or aqueous alteration, several fgMMs contain either unusually high abundances of euhedral enstatite and/or forsterite within a fine-grained matrix or have spatial variations in Fe-content within their fine-grained matrix suggesting these contain pseudomorphs of pre-existing euhedral crystals. Similar textures are observed within intensely aqueously altered CM2 chondrites such as Cold Bokkeveld and are hydrated chondrules [5].

Discussion: The relative abundances of unmelted MM types suggest there are four main parental sources: (1) a C1 asteroidal source, which has experienced intense aqueous alteration, (2) a C2 asteroidal source containing chondrules that has experienced less aqueous alteration, (3) a C3 source that has experienced little compaction and minor aqueous alteration, and (4) a chondrule-dominated unequilibrated source.

Although three of these sources have affinities to CI1, CM2/CR2 and ordinary chondrites their mineralogies and textures differ in detail. Transmission electron microscope studies of fgMMs indicate that the clay mineral smectite dominates MM matrices [9, 10, 11] whilst serpentine or serpentine-smectite interlayed clay minerals dominate CI1 and CM2 chondrite matrix [5]. Pyroxene is also the most abundant anhydrous silicate found amongst MMs, whilst olivine dominates within most of the chondritic meteorite groups. These differences indicate that chondritic meteorites and MMs sample different asteroidal parent bodies.

The discrete oxygen isotope abundances of chondritic meteorite groups are often considered as evidence that these are not derived from a single heteorogeneous parent body [5]. A recent study of the oxygen isotope systematics of MMs likewise indicates a wide range of values, however, these are also not consistent with those of meteorites [12].

The presence of highly porous C3 particles is anomalous. These materials have some affinities with the matrices of CR2 chondrites since these also contain framboidal magnetite, include areas that are relatively porous and have experienced a low degree of aqueous alteration. They are also broadly similar to hydrated interplanetary dust particles. The discovery of isotopically anomalous presolar silicates within MMs, CR2 matrix and IDPs [13, 14] may suggest a genetic link between all three groups of materials. The occurrence of an oxidized (Type II) chondrule fragment within one C3 particle in the current study, however, implies that the materials have an asteroidal source, albeit one that may be transitional to comets.

Implications: The results of this study indicate that MMs are derived from at least 4 principal types of parent body, all of which are likely to be asteroids but differ from those of meteorites. Athough it is impossible to determine at present whether meteorite parent bodies are sampled by MMs, it is clear that meteorites do not sample parent bodies representative of the predominant sources of MMs. It is clear that meteorites and/or MMs are a highly biased sample of the main asteroid belt.

References:[1] Maurette M. M. et al., (1991) *Nature*, 351, 44-47. [2] Kortenkamp S. J. & Dermott S. F. (1998) *Icarus*, 135, 469-495. [3] Nesvorny D. et al., (2004) *Astrophys. J.*,591, 486-497. [4] Genge M. J. et al. (1997) *GCA,61*, 5149–5162. [5] Brearley A. J. & Jones A. P. (1998) *Reviews in Min*, 36, 1-191. [6] Gounelle et al. (2005) *Science*, in press. [7] Genge M. J. (2005) *MAPS* (Feb delayed). [8] Genge M. J. (2004) 35th *LPSC*, abs 1102. [9] Nakamura T. et al., (2001) GCA, 65(23), 4385-4397. [10] Noguchi T. et al. (2002) *EPSL*, 202(2), 229-246. [11] Genge M. J. et al. (2001) 32nd *LPSC*, abs. 1546. [12] Matrajt et al. (2005) *This conference*. [13] Yada T. et al. (2005) 36th *LPSC*, abstract 1227. [14] Kobayashi S. et al., (2005) 36th *LPSC*, abstract 1931.

DEVELOPMENTS IN THERMAL ANALYSIS OF LABILE TRACE ELEMENTS IN CARBONACEOUS CHONDRITES.

Julia S. Goreva and Dante S. Lauretta, University of Arizona, Lunar and Planetary Laboratory, Tucson

Introduction and technique. Abundances and isotopic compositions of the labile chalcophile and siderophile elements (in order of increasing condensation temperature – Hg, Cd, Tl, In, Bi, Pb, S, Te Se Zn Sn, Ge, Sb, Ga, Na, Ag, As, Au, Fe) in primitive materials reflect low temperature gas-solid interactions in the early solar system. Most of these volatile, non-ice-forming elements are predicted to initially condense as a trace element in the bulk metal phase; others are transferred during metal sulfurization [1, 2]. Because of their high volatility and their mobility in aqueous systems, these elements may be excellent indicators of the low-temperature, thermal and hydrological processes experienced by primitive chondritic meteorites and cometary particles.

Here we present results using new, thermal-analysis (TA-) ICP-MS technique. By coupling a home-built inductively heated programmable furnace with a high-resolution ICPMS, we are able to simultaneously measure the thermal release profiles of elements from small samples. This technique is essentially an advanced thermogravimetry method. Isotopically pure ^{200}Hg spike solution supplied into the furnace from cold-vapor generator is used to optimize the system performance and as an internal standard during heating experiments.

A series of heating experiments were performed on a suite of CI, CM, CV, and CO carbonaceous chondrites. Small aliquots of the meteorite powders were heated from room temperature to 1100 °C under an inert Ar atmosphere. For the external quality control of the bulk chemical abundance of the trace elements of interest we have use certified standard reference materials JG-1 Granodiorite and JB-2 Basalt as well as the Allende meteorite reference sample. Acid dissolution of both heated and pristine aliquots of standards used as a control on the amount of liberated material.These experiments allow us to determine the bulk abundances of labile elements, and their distribution among different (mostly S-bearing phases).

Results. Typical element release profiles during the heating experiments for different carbonaceous chondrite classes are plotted in Fig.1.

CI chondrites (Orgueil) releases detectable quantities of S over the entire temperature range with distinct maxima at 250, 500, and 650 °C (Fig. 1a). Low amounts of As and Sb are liberated. Significant quantities of Se, Cd, Te, and Hg are detected with correlated maxima in S, Se, and Te release profiles at 250 and 500 °C. The release of S, As, Se, Cd, and Te reach maxima at 650 °C.

CM chondrites continuously release S at temperature greater than 100 °C. There are maxima in the S-release profiles at 300°C and 600 °C (Fig. 1b). They release small amounts of As above 700 °C with maxima at 400 °C. Selenium is released continuously from the CM chondrites at temperatures above 200 °C with maxima at 400 °C. There are maxima in the Cd-release between 700 and 800°C. Antimony and Te are released at low levels throughout the entire duration of the experiments. There are sharp peaks in the Te-release at 725 °C.

CV chondrites release significantly less S compared to the CM chondrites There are two maxima in the S-release profile from Allende (CV) and Grosnaja (CV) at 320 and 420 °C. Continuous S release occurs above 500 °C. Sulfur release from Mokoia (CV) begins at 200 °C with a maxima at 500 °C. Vigarano (CV, Fig. 1c) is distinctly different. The majority of S is released at 400 °C and continues to release throughout the experiment. The maxima in the S release profiles from Allende (CV), Mokoia (CV), and Grosnaja (CV) correlates with ones in the As and Se profiles. The maxima in the Vigarano (CV) S-release profile is perfectly correlated with those in the As, Se, and Te profiles. There are peaks in the Cd release profiles from Allende, Mokoia, and Vigarano between 675 - 700 °C.

CO chondrites do not release detectable amounts of S below 500 °C (Fig. 1d). The release of As, Se, Cd, Sb, and Te reach maxima between 300 and 400 °C from Kainsaz (CO). The release pattern from Ornans (CO) is distinctly different. Very little material is liberated below 800 °C. The release of S and Se is correlated. Isna (CO) releases Se, Sb, and Hg at low T and has a S-release pattern that is similar to Kainsaz. It releases Sb between 350 and 550 °C. The peak release for Cd and Te occurs above 900 °C.

Interpretation and application to Stardust. There is a low-temperature S-bearing phase in the CI, CM, and CV carbonaceous chondrites, which is absent in the CO chondrites. These results place constraints on the origin and thermal history of volatile elements in these meteorites. The bulk abundances are the result of condensation processes in the solar nebula. Subsequent alteration on the

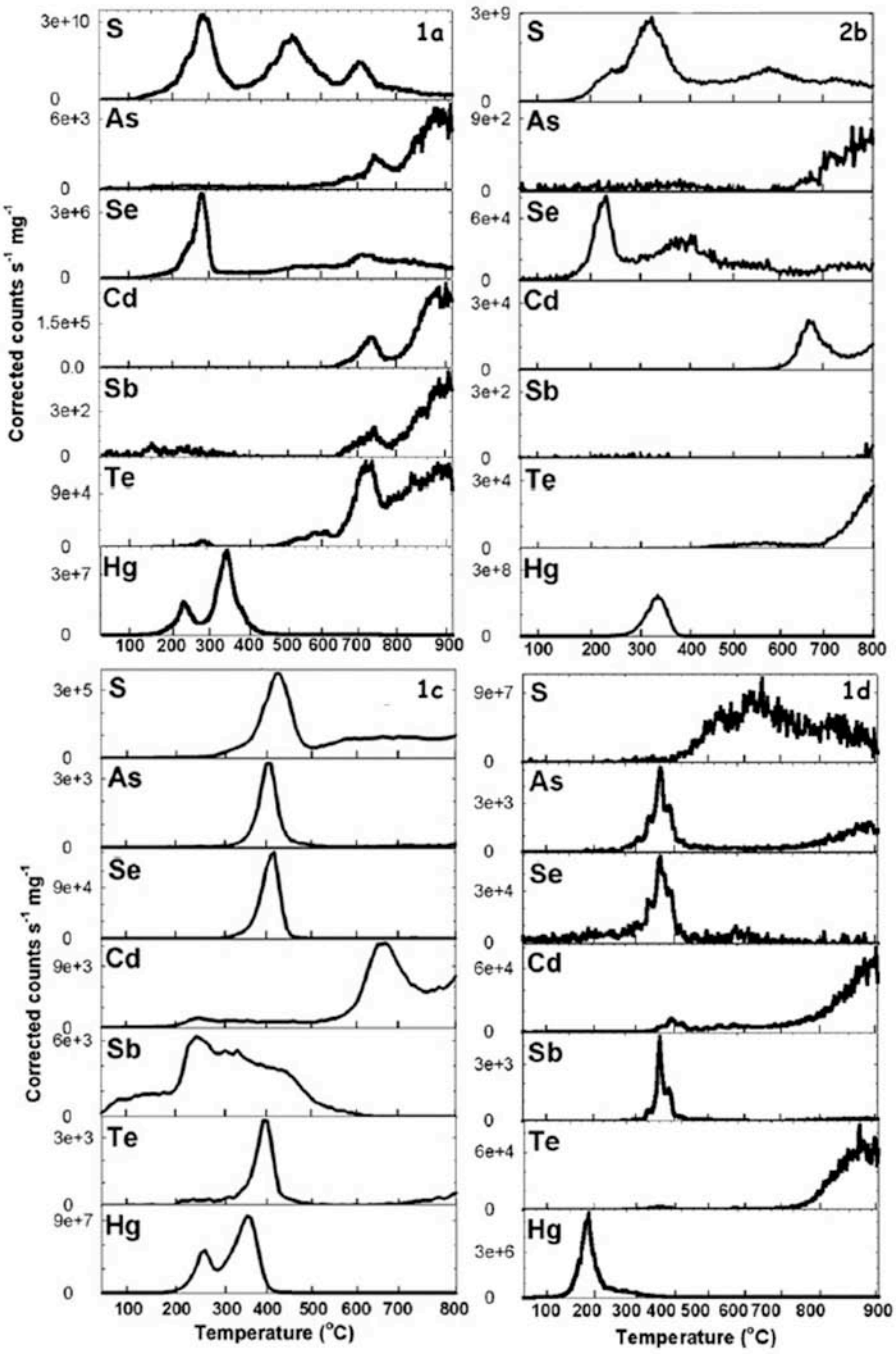

Figure 1. Thermal release profiles for 1a Orgueil (CI), 1b Murchison (CM), 1c Vigarano (CV) and Kainsaz CO)

meteorite parent bodies likely redistributed the trace elements into low-temperature phases. This redistribution had a significant effect on the rate and extent of volatile loss during thermal metamorphism.

Since the amount of the material required for analyses is very small and techniques is non-destructible with respect to silicates and metals, it can be applied to Stardust particles prior to other chemical and isotopic analyses. Moreover, labile elements are excellent indicators of the heating and volatile loss experienced by Stardust samples as they passed through the aerogel. Investigation of the volatile abundances along the particle tracks may help to determine the order in which different trace elements were released and a degree of heating.

Ref. [1] Lauretta et al. (2002) *LPSC, XXXIII*, 1602. [2] Lodders and Fegley (1998) *The Planetary Scientist's Companion, Oxford*

GREAT EXPECTATIONS – DUST RECOVERED FROM AEROGEL. G. A. Graham[1], J. P. Bradley[1], Z. R. Dai[1], A. T. Kearsley[2], M. Bernas[3] and C. Snead[4], [1]Institute of Geophysics & Planetary Physics, Lawrence Livermore National Laboratory, CA 94551, USA (graham42@llnl.gov), [2]Mineralogy Department, The Natural History Museum, London SW7 5BD, UK, [3]Applications Laboratory, FEI Company, OR 97124, USA, [4]Space Sciences Laboratory, University of California at Berkeley, CA 94720, USA.

Introduction: Cometary dust particles captured during the flyby of comet 81P/Wild-2 by NASA's Stardust spacecraft will be returned to Earth in January 2006 [1-2]. One of the fundamental questions to be answered in the preliminary examination is whether the captured particles are similar to the current materials studied in the laboratory, i.e. interplanetary dust particles (IDPs). From detailed IDP studies it is assumed that anhydrous particles are from cometary bodies [3] and hydrous particles are from asteoridal bodies [4].

Although the stratospheric collection of IDPs results in the capture of material in a near-pristine state, significant heating is extensive in all particles [5]. This is in stark contrast to Stardust, where the cometary particles have embedded into the low-density silica aerogel collectors at ~6.1 km s^{-1}. Previous studies have shown that hypervelocity impact (HVI) capture of dust can result in fragmentation, thermal and shock alteration [6] even when the substrate is a low density material [7].

In the build-up to Stardust, several laboratory studies have accelerated analogue projectiles (e.g. single mineral grains and meteorite fragments) into aerogel targets at encounter velocities to investigate the effects of HVI capture [8-9]. In addition to these laboratory materials, NASA's Orbital Debris Collection (ODC) experiment exposed 0.63 m^2 of 0.02g cm^{-3} silica aerogel on the Mir space station for 18 months [10]. Recent studies of impacts extracted from ODC aerogel tiles have focused on in-situ mapping [11-12]. While these studies highlight the degree of fragmentation, they only enable the acquisition of bulk chemical or elemental data so it is not possible to directly observe structural or mineralogical alteration that would be comparable to IDPs. In this study we report on the composition of individual particles extracted from the terminal point of impacts.

Methods: The particles were isolated from the bulk aerogel using glass micro-needles. The particles were subsequently mounted onto standard SEM pin-stubs using carbon adhesive tabs.

Preliminary SEM/EDX Screening. A JEOL 5900 LV SEM fitted with an Oxford Inca EDX system was used to confirm extraterrestrial origin. The particles were then subjected to X-ray mapping to identify the location of molten aerogel which adheres to the surface of the particle during the HVI capture.

FIB Lift-out. Electron transparent sections of the terminal particles were produced using focused ion beam (FIB) milling in an FEI DB237 FIB/FESEM tool fitted with STEM and EDAX Genesis EDS detectors [13].

TEM Analysis. A CM300 Field Emission Gun Transmission Electron Microscope (FEGTEM) fitted with an Oxford X-ray energy dispersive spectrometer was used to characterize the FIB sections.

Results & Discussion: Any particle collector exposed in low-Earth-orbit will also contain impacts generated by artificial orbital debris. As a result, all of the particles used in this study were from the so-called "chondritic swarm" impacts [10]. Preliminary secondary electron imaging in the SEM showed that all of the particles had the characteristic molten aerogel coating on the surface of the grains (Figure 1). This has been seen on all previously studied ODC particles [10] and in particles extracted from laboratory impacts [9]. This molten aerogel is essentially a fusion layer most likely formed during the initial collision between the whole particle and the substrate. A significant benefit of using FIB microscopy to prepare the electron transparent sections (~100 nm) is that precise sections can be made that are nearly free of the molten aerogel which would have contaminated any detailed mineralogical or chemical analyses.

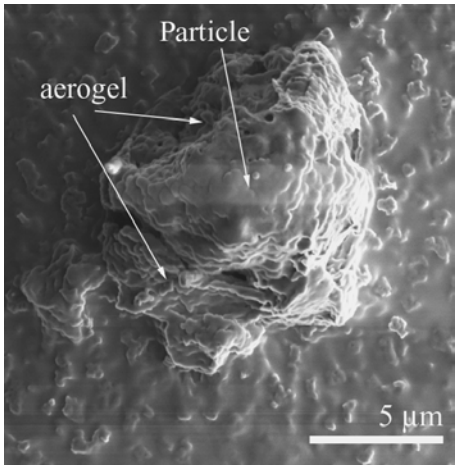

Fig.1: Secondary electron image of a terminal particle extracted from aerogel. The particle diameter is ~7 µm.

Figure 2 shows a 30 kV SEM-STEM bright-field image of one of the terminal particles. Unlike the previous study of the chondritic swarm particles [10] the section does not show extensive evidence of aerogel penetrating into the bulk particle. Detailed TEM investigation of the particle section identified the major mineral component to be serpentine with additional minor phases including spinel. This is a different mineral assemblage to that originally identified in the chondritic swarm particles where the major phase was olivine [10]. However as the swarm particles are proposed to have been generated by a grazing impact of a larger chondritic mass on the space station, it is not unreasonable that the composition of the particles captured is varied. In addition to the characterization of the mineralogy of the terminal particle, the TEM study revealed that extensive thermal alteration had occurred to the rim of the particle evident by the amorphous material and the vesicular texture. It can be argued from the observations made on ODC particles that they are not analogues of Stardust particles as the HVI speeds of capture were in excess of 10 km s^{-1} compared to 6.1 km s^{-1}. Therefore higher degrees of alteration could be expected. However, the observations made on the ODC particles are similar to those seen in recent laboratory impact simulations at ~2-6 km s^{-1} where vesicular and amorphous material was observed at the rims of the mineral grains while the cores were relatively pristine [9,15].

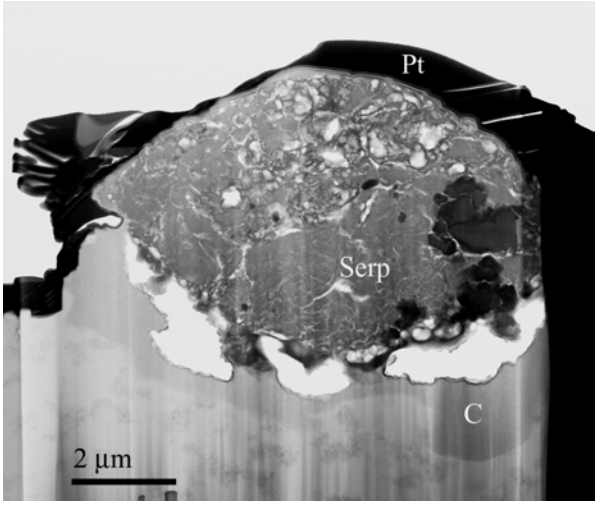

Fig.2: 30 kV SEM-STEM bright-field image of the terminal particle FIB section.

Both theoretical modeling [14] and synchrotron x-ray mapping studies of ODC impacts [11-12] suggest a high degree of fragmentation will be observed in Stardust impacts. As a consequence, it can be argued that the terminal particles will only represent the most robust grains. However both in this study and the previous study of extraterrestrial terminal grains extracted from the ODC tiles [10], the compositions have been found to be polymineralic.

Conclusions: The terminal particles showed clear evidence of vesiculation and alteration of mineralogy at the rims; however, in at least one of the particles, the core appeared relatively unaltered. Therefore, while it is likely that Stardust particles will have undergone degrees of alteration during capture, at least some of the material within the particles will be in a relatively pristine state. So while it is likely that Stardust particles will not be as pristine in nature as IDPs there will still be significant unaltered material to investigate and compare with the current meteoritic collections.

References: [1] Brownlee D. E. et al. (2004) *Science, 304,* 1764-1769. [2] Tuzzolino A. J. et al. (2004) *Science, 304,* 1776-1780. [3] Bradley J. P. and Brownlee D. E. (1986) *Science*, 231, 1542-1544. [4] Bradley J. P. and Brownlee D. E. (1991) *Science,* 251, 549-552. [5] Bradley J. P. (2005) *Pers. Comm*. [6] Graham G. A. et al. (2001) *IJIE*, 26, 263-274. [7] Burchell M. J. et al. (1999) PSS, 47, 189-204. [8] Burchell M. J. et al. (2001) *MAPS*, 36, 209-221. [9] Okudaira K. et al. (2004) *ASR*, 34, 2299-2304. [10] Hörz F. et al. (2000) *Icarus*, 147, 559-579. [11] Borg J. et al. (2004) *LPS XXXV*, Abstract #1580. [12] Ishii H. A. et al. (2004) *LPS XXXVI*, Abstract #1387. [13] Graham G. A. et al. (2004) *LPS XXXV*, Abstract #2044. [14] Okudaira K. et al. (2005) *LPS XXXVI*, Abstract #1832. [15] Anderson W. W. and Ahrens T.J. (1994) *JGR*, 99, 2063-2071.

Acknowledgement: This work was in part performed under the auspices of the U.S. Department of Energy, National Nuclear Security Administration by the University of California and Lawrence Livermore National Laboratory under contract No.W-7405-Eng-48. This work was performed as part of the Bay Area Particle Analysis Consortium (BayPAC). GAG, JB and ZRD are supported by NASA grant NNH04AB49I and CS is supported by NASA grant NAG5-119. F. Hörz (NASA JSC) is thanked for the supplying the ODC tiles used in this study.

GEO DEBRIS AND INTERPLANETARY DUST: FLUXES AND CHARGING BEHAVIOR. A. L. Graps[1], S. F. Green[2], N. M. McBride[2], J. A. M. McDonnell[3], G. Drolshagen[4], H. Svedhem[4], K. D. Bunte[5]
[1]Institute of the Physics of Interplanetary Space (IFSI), CNR-ARTOV, Via del Fosso del Cavaliere 100, 00133 Rome, Italy. Amara.Graps@ifsi.rm.cnr.it, [2]The Open University, UK, [3]Unispace Kent, UK, [4]ESTEC, The Netherlands, [5] eta_max space, Germany

Introduction: A population of cosmic dust mixed with a population of man-made debris exists within the Earth's magnetosphere. Measurements of these provide the data samples for studies of the interplanetary dust particles that travel through our magnetosphere from the outside, and for studies of the local byproducts of our space endeavours. Even though instruments to detect natural meteoroids and space debris particles have been flown in Low Earth Orbits (LEO) and on interplanetary missions, very little information on the particle environment for Earth orbits above about 600 km altitude have been available. In particular, knowledge about particles smaller than 1 m in the geostationary (GEO) region was largely unknown before GORID [1]. In September 1996, a dust/debris detector: GORID, was launched into GEO as a piggyback instrument on the Russian Express-2 telecommunications spacecraft. The instrument began its normal operation in April 1997 and ended its mission in July 2002. The goal of this work was to use GORID's particle data to identify and separate the space debris from the interplanetary dust particles (IDPs) in GEO, to more finely determine the instrument's measurement characteristics and to derive impact fluxes. Here we present results of that study.

Clustering: Very large variations in daily event rates led to the identification of clusters of events, some of which re-occurred on consecutive days at the same local time [1,2]. They were interpreted as clouds of aluminium oxide debris resulting from the firing of solid rocket motors. Clustering of events is therefore indicative of a debris source and provides a selection criteria for statistical separation of the debris and IP populations. The mean rate for science events is 1.83 day^{-1} corresponding to an interval of 0.55 d. The distribution of times between events shows a bimodal distribution with one component peaking at about the expected “random” rate and the other with very much shorter times, indicating clustering. The limit of cluster membership is consequently defined at 0.05 days.

The temporal and charge distributions: Debris are concentrated near midnight local time except during summer. In early summer, clustered events are concentrated near 5 am, just at the time when beta-meteoroids may be expected to be detected. The GORID pointing geometry implies preferential detection of debris after recent crossing of the equatorial plane in the magnetotail. This may be because debris are physically constrained to this region or because some process in the magnetosphere, such as a charging mechanism, makes them more detectable. One possible mechanism leading to the clustered events is electrostatic fragmentation of the slag particles, after passing through the current sheet.

The detection rate and fluxes: The detection rate of interplanetary events is 0.54 d^{-1} and debris events is 2.46 d^{-1}. The fluxes of interplanetary particles are reasonably close to the well-defined model prediction, allowing for the impact speed uncertainty. The mean fluxes are 1.35×10^{-4} m^{-2} s^{-1} for IP and 6.1×10^{-4} m^{-2} s^{-1} for debris at the detection threshold of $Q_i = 1.3 \times 10^{-13}$ C. The flux of space debris detected by GORID appears to be higher than in LEO although the results are sensitive to the assumed speeds.

References:

[1] Drolshagen, G., Svedhem, H., Grün, E., Grafodatsky, O., and Prokopiev, U. (1998). “Microparticles in the Geostationary Orbit (GORID Experiment)”, COSPAR 98, B0.2 – 0014. [2] Svedhem, H., Drolshagen, G. Grün, E. Grafodatsky, O. and Prokopiev, U. (2000). “New results from in-situ measurements of cosmic dust – Data from the GORID experiment”, Adv. Space Res. 25, 309-314.

STARDUST WILD 2 DUST MEASUREMENTS. S. F. Green[1], N. McBride[1], M. T. S. H. Colwell[1], J. A. M. McDonnell[1], A. J. Tuzzolino[2], T. E. Economou[2], B. C. Clark[3], Z. Sekanina[4], P. Tsou[4], D. E. Brownlee[5], [1]PSSRI, The Open University, Walton Hall, Milton Keynes, MK7 6AA, UK, s.f.green@open.ac.uk, [2]Laboratory for Astrophysics and Space Research, Enrico Fermi Institute, University of Chicago, 933 East 56th St, Chicago Ill 60637, USA, [3]Jet Propulsion Laboratory, California Institute of Technology, 4800 Oak Grove Drive, Pasadena CA 91109, USA, [4]Lockheed Martin Astronautics, P.O. Box 179, MS-B0560, Denver, CO 80201, USA, [5]Astronomy Department, University of Washington, bx 351580, Seattle, WA 98195, USA.

Introduction: The Stardust Dust Flux Monitor Instrument (DFMI) detected almost 9000 dust impacts over a broad mass range of 10^{-14} to 10^{-6} kg during the 236 km flyby of comet 81P/Wild 2 on 2 January 2004. Cometary dust particles, trapped in the volatile ices of the nucleus since their formation, contain information on the conditions in the pre-solar nebula, its precursor interstellar cloud and nucleosynthetic processes in the stars from which their constituent grains originally formed. The primary objective of Stardust is to capture these samples intact and return them to the Earth for in-depth microanalysis [1]. These dust grains are the source of a major component of interplanetary dust and large (sub-mm and larger) grains are observed in cometary dust trails forming relatively long lasting meteoroid streams, which gradually dissipate into the zodiacal dust complex. Micron sized (and somewhat smaller) grains can be swept out of the inner solar system by solar radiation pressure. The contribution of comets to the total interplanetary dust complex, and the subsequent dynamics of the individual grains, are critically dependent on the dust mass (or size) distribution. Furthermore, the dust-to-gas ratio in cometary nuclei provides constraints on the conditions in the region in which it formed. DFMI provided time resolved dust fluxes and mass distributions in the inner coma of comet Wild 2 at the highest resolution yet obtained.

DFMI: The DFMI [2] combines small area but high sensitivity PVDF (polyvinylidene fluoride) sensors with two piezoelectric acoustic sensors, mounted on the first two layers of the spacecraft Whipple dust shield, to measure the flux of larger particles. The PVDF sensors each had four mass channels with thresholds from 10^{-14} kg (particle radius ~ 3 μm) to 10^{-7} kg. The front shield acoustic sensor could detect particles of mass larger than 3×10^{-11} kg (~50 μm diameter), while the second sensor detected penetrating particles of mass $> 2 \times 10^{-7}$ (~ 1 mm diameter).

The objectives of the Stardust Dust Flux Monitor Instrument (DFMI) were to:

1) Measure the interplanetary dust flux,
2) Determine particle fluxes during the 81P/Wild 2 flyby,
3) Determine the particle mass distribution in the coma of 81P/Wild 2,
4) Provide the context for the collected dust samples,
5) Monitor the dust environment at P/Wild 2 for spacecraft health and interpretation of anomalies.

Although an unidentified noise source prevented interplanetary cruise measurements, the instrument worked flawlessly throughout its 30 minutes of operation in the inner coma of comet Wild 2.

DFMI Encounter measurements: The first dust detections were made by the front shield acoustic sensor, 264 s before closest approach (at a cometocentric distance r = 1630 km). The event rate gradually increased up to closest approach and then decayed afterwards with a second period of high activity between +620 s (r = 3810 km) and +720 s (r = 4420 km). The last detected particle was at +922 s at a cometocentric distance of r = 5650 km [3].

The spatial distribution of dust was highly non-uniform, with short duration bursts of impacts implying localized spatial density changes of orders of magnitude on scales of less than a km [3]. Long exposure images of the comet reveal large numbers of jets projected nearly around the entire perimeter of the nucleus, many of which appear to be highly collimated, with angular sizes of a few degrees [4].

The overall mass distribution in the inner coma is dominated by the largest grains, with an average cumulative mass distribution index of $\alpha = 0.75 \pm 0.05$ (where the number of particles of mass m or larger, $N(m) \propto m^{-\alpha}$). However, the mass distribution was also highly variable during the flyby and almost 80% of the detected impacts occurred during the second period of high activity, ~4000 km from the nucleus, where small grains dominated, with $\alpha = 1.13 \pm 0.2$ [5].

Jets and Fragmentation: The detection rates are characterized by structure on timescales of seconds ('swarms' with spatial scales of 10s of km) and fractions of a second ('bursts' with spatial scales of less than 1 km) [3].

The swarms have dimensions consistent with the jets seen in the Stardust NAVCAM images. Many of the swarms can be correlated with the positions of jets [6] although definitive solutions are not possible due to lack of knowledge of the nucleus rotation rate and grain terminal velocities.

The enormous variations in dust spatial density over distances of a few hundred metres, which characterize the bursts, cannot be explained by grain dynamics within the coma, particularly as they occur outside the innermost coma, where gas drag is no longer the dominant force. Particle fragmentation provides the only viable explanation [3],[5],[7]. The bursts result from the passage of Stardust through expanding dust clouds resulting from extended fragmentation. The second period of high activity results from outgassing and/or fragmentation of a large (10s of metres diameter) boulder [6].

The interpretation of this highly structured coma as due to a combination of jets and particle fragmentation has been received with some skepticism. The evidence will be reviewed and common criticisms refuted. Comparisons with results from The P/Halley and P/Grigg-Skjellerup flybys indicate that the same processes occurred in both comets for which in-situ dust data are available and therefore may be common in comets in general.

References:

[1] Brownlee D. E. et al (2003) *JGR, 108,* SRD-1, 1-12. [2] Tuzzolino A. J. et al. (2003) *JGR, 108,* SRD-5, 1-24. [3] Tuzzolino A. J. et al. (2004) *Science*, *304*, 1776-1780. [4] Brownlee D. E. et al (2004) *Science 304*, 1764-1769. [5] Green S. F. et al. (2004) *JGR, 109,* E12SO4, 1-13. [6] Sekanina Z. et al. (2004) *Science*, *304*, 1769-1774. [7] Clark B. C. et al. (2004) *JGR*, *109*, E12SO3, 1-13.

PROSPECTS OF DUST A ASTRONOMY MISSION. E. Grün[1,2], R. Srama[1], S. Helfert[1], S. Kempf[1], G. Moragas-Klostermeyer[1], M. Rachev[1], A. Srowig[1], S. Auer[3], M. Horanyi[4], Z. Sternovsky[4], and D. Harris[2], [1]MPI-K, Heidelberg, Germany, [2]HIGP, Honolulu, USA, [3]A&M Assoc., Basye, USA, [4]LASP, Boulder, USA

Dust particles, like photons, carry information from remote sites in space and time. From knowledge of the dust particles' birthplace and their bulk properties, we can learn about the remote environment out of which the particles were formed. This approach is called "Dust Astronomy" which is carried out by means of a dust telescope on a Dust Observatory in space.

There are different types of dust particles in interplanetary space: dust from comets and asteroids and interstellar grains traversing the solar system. The most obvious sources of interplanetary dust are comets which move on highly excentric orbits through the solar sytem. A significant fraction of meteors and dust grains in the zodiacal cloud have their origin in the asteroid belt. Their orbits have low inclinations and low eccentricities which allows for a distinction from fresh cometary dust which moves on highly eccentric orbits.

Galactic dust grains passing through the planetary system have been positively identified at Jupiter's distance by the dust detector onboard the Ulysses spacecraft. Analysis of data obtained within and beyond the Earth orbit by different spacecraft (Helios, Galileo, and Cassini) show that a significant amount of ISD is at our reach. The motion of interstellar grains through the solar system is parallel to the flow of neutral interstellar hydrogen and helium gas, both traveling at a speed of 26 km/s.

So far, a clear identification of the origin of cosmic dust near Earth was not possible. Especially, the origin of Interplanetary Dust Particles (IDPs) collected in the Earth's stratosphere and extracted from Antarctic ice is still unclear. These are the only cosmic dust grains which are currently accessible for laboratory analysis. By simultaneously measuring in-situ the particles' trajectories in space and their chemical composition we will distinguish interstellar from cometary and asteroidal dust grains and obtain important cosmochemical information.

In interplanetary space the expected impact rate on dust detectors at 1 AU is low, e.g. an impact detector of 0.1 m^2 sensitive area records only about 1 particle of 10^{-13} g (0.2 μm radius) per day and 1 particle of 10^{-10} g (2 μm radius) per two weeks, respectively. Therefore, a dust telescope needs to have at least 0.1 m^2 sensitive area.

Any meteoroid in interplanetary space is electrically charged. Because of the predominance of the photoelectric effect in interplanetary space, meteoroids are usually charged at a potential U of about +5 Volts. In near-Earth environment (LEO) the low energy plasma prevails leading to dust grain potentials of about -0.5 V whereas in the highly variable high energy plasma regime at geostationary distance dust potentials from -30 V to +3 V are expected. It was Cassini's CDA [1] instrument that for the first time reliably identified this dust charge ($\geq 10^{-15}$ C corresponding to ~ 2 μm radius) in interplanetary space [2]. From the signal the speed and impact direction was determined.

Compositional analyses of cometary dust have been achieved by the dust mass analyzers, PIA and PUMA on board spaceprobes to comet Halley [3]. The instruments employed a time-of-flight mass spectrometer in order to obtain the elemental composition of the plasma generated upon impact of cometary dust particles onto the sensor. A mass resolution of $M/\Delta M > 100$ was achieved by the use of a reflectron that provided energy focusing. Because of the very high dust fluxes expected near the comet only a very small sensitive area of 5 cm^2 was necessary to obtain thousands high resolution dust mass spectra. The data collected by PIA/PUMA demonstrate that each individual event detected contains a wealth of scientific information.

The Stardust spacecraft carrying the Cometary and Interstellar Dust Analyzer instrument, CIDA, flew by comet Wild 2 in 2004. CIDA, too, is an impact mass analyzer employing a reflectron stage in order to provide high resolution ($M/\Delta M > 100$) mass spectra. The sensitive area of this instrument is 90 cm^2. CIDA provided compositional analyses of a few tens of cometary [4] and of presumably interstellar grains [5]. Krueger et al. conclude that the main constituents of interstellar grains are organic with a high oxygen and low nitrogen content.

Based on experience with current space dust instruments a novel dust telescope is being developed. It is optimized for (1) large area (0.1 to 1 m^2) impact detection and trajectory analysis of submicron-sized and larger dust grains, (2) the determination of physical properties of sub micron sized grains, such as flux, mass, speed, electrical charge, and (3) high resolution chemical analysis ($M/\Delta M \geq 100$) of cosmic dust. A plasma monitor supports the dust charge measurements.

A dust telescope is a combination of a dust trajectory sensor (Fig. 1) together with an analyzer for the

chemical composition of dust particles in space. Dust particles' trajectories are determined by the measurement of the electric signals that are induced when a charged grain flies through a position sensitive electrode system. The objective of the trajectory sensor is to measure dust charges in the range 10^{-16} to 10^{-13} C and dust speeds in the range 6 to 100 km/s. First tests with a laboratory set-up have been performed and demonstrate the expected performance. An ASIC charge sensitive amplifier and an ASIC transient recorder has been developed with a RMS noise of about 1.5 10^{-17} C.

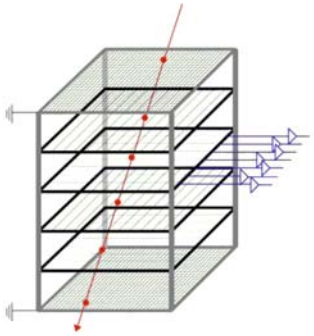

Fig. 1 Schematics of the Dust Trajectory Sensor

The dust chemical analyzers (Fig. 2) has sufficient mass resolution in order to resolve ions with atomic mass numbers up to 100. The annular impact area of the mass analyzer will be more than 0.1 m^2. The mass spectrometer consists of the target area with an acceleration grid and the single-stage reflectron consisting of two grids and the central ion detector. An ion detector of 50 to 110 mm radius is necessary to collect all generated ions. A lab model has been constructed and first dust accelerator show that a mass resolution of $M/\Delta M > 150$ can be obtained for impacts onto the target.

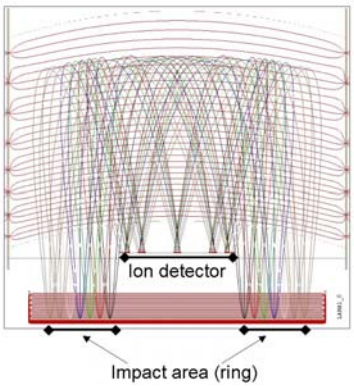

Fig. 2 Schematics of the Large-Area Mass Analyzer showing ion trajectories from different impact positions and equal potential lines.

A Dust Astronomy Mission named Cosmic DUNE is being proposed. It establishes the next logical step beyond NASA's Stardust mission, with four major advancements in cosmic dust research: (1) Analysis of the elemental and isotopic composition of individual cosmic dust grains, (2) determination of the size distribution of interstellar dust, (3) characterization of the interstellar dust flow through the planetary system, and (4) analysis of interplanetary dust of cometary and asteroidal origin.

The mission scenario and measurements requirements has been studied using the small European ConeXpress platform with solar electric propulsion for transport to an halo orbit around L2. ConeXpress is three axis stabilized and provides a pointing accuracy better than the 1°. The power demand of the instruments is largely covered by the electrical power provided by the solar arrays. The first half of the mission consists in reaching the Moon in order to prepare for a Moon flyby that, in turn, deflects the spacecraft into an orbit around the L2 point. The second half of the mission scenario consists in a Moon flyby, preparing the insertion of the spacecraft into a Halo orbit around L2.

Cosmic DUNE is well suited to investigate the micro meteoroid environment in interplanetary space or in the near-Earth environment. For the first time, this instrument will allow us the in-situ analysis of the properties of micron sized particles together with the identification of its source. Cosmic DUNE will prepare the way for effective collection in near-Earth space of interstellar and interplanetary dust for subsequent return to Earth and analysis in laboratories.

[1] Srama, R., et al., 2004b, ESA-SP 543, 73-78. [2] Kempf, S., et al., 2004, Icarus, 171, 317-335. [3] Kissel, et al., 1986, Nature 321, 336-338. [4] Kissel, J., Krueger, F.R., Silen, J., Clark, B.C., Science, 304, 1774-1776, 2004. [5] Krueger F. R. et al., Rapid Comm. Mass Spectrom. 18, 103 (2004).

DUST PARTICLES DETECTED IN THE OUTER SOLAR SYSTEM BY VOYAGER 1 AND 2.

D. A. Gurnett, Z. Z. Wang, A. M. Persoon, and W. S. Kurth (University of Iowa, Dept. of Physics and Astronomy, Iowa City, IA 52242, USA; donald-gurnett@uiowa.edu)

In this paper we report PWS observation of dust impacts detected in the outer solar system by the Voyager 1 and 2 plasma wave instruments. During the Voyager 1 and 2 flybys of the outer planets, it was discovered that the plasma wave (PWS) instrument could detect small micron-sized particles striking the spacecraft. When a small particle strikes the spacecraft at a high velocity, the particle is instantly vaporized and heated to a very high temperature, typically 10^4 K, or more. At this high temperature a substantial fraction of the gas is ionized. As the resulting plasma cloud sweeps over the PWS electric antenna, it produces a voltage pulse on the antenna. By counting the number of pulses per unit time, the impact rate can be determined.

An example of a dust impact detected by Voyager 2 at a heliocentric radial distance of 53.62 AU (Astronomical Units) is shown in Figure 1. Typically the voltage pulse detected on the antenna consists of an abrupt step with a rise time of a few tens of microseconds followed by complicated recovery waveform lasting several milliseconds.

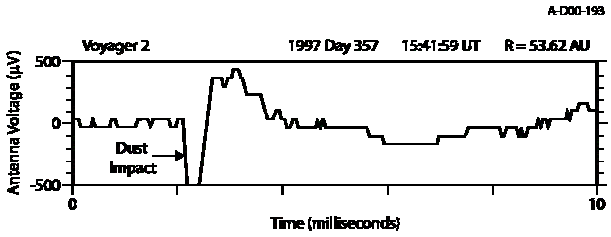

Figure 1. A dust impact detected by the Voyager 1 plasma wave instrument at a heliocentric radial distance of 53.62 AU.

The waveforms detected in interplanetary space are very similar to the waveforms detected at the Saturn ring plane crossings, which are believed to be due to micron-sized particles. After eliminating dust impacts detected during the flybys of the outer planets, the impact rates detected by Voyagers 1 and 2 are found to be nearly constant, approximately 4 impacts per hour for Voyager 1, and 5 impacts per hour for Voyager 2, after correcting for the observation duty cycle. Plots of the impact rates detected by Voyagers 1 and 2 are shown in Figures 2 and 3, respectively.

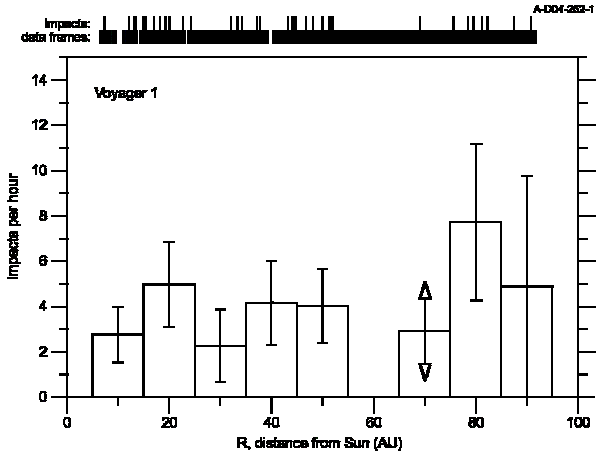

Figure 2. The dust impact rate detected by the plasma wave instrument on Voyager 1.

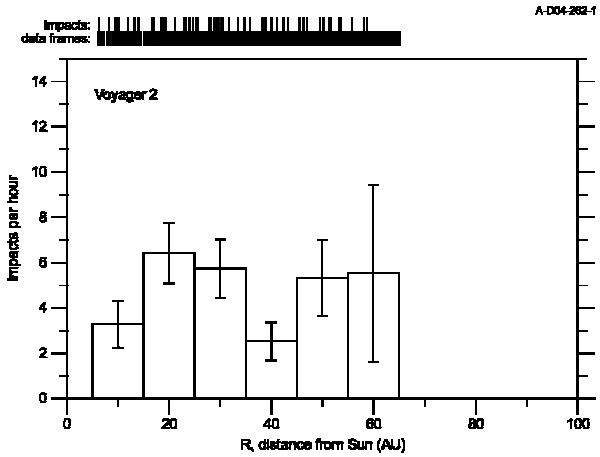

Figure 3. The dust impact rate detected by the plasma wave instrument on Voyager 2.

The impact rates shown in Figures 2 and 3 appear to be completely independent of the heliocentric radial distance of the spacecraft. Voyager 1 is currently at a heliocentric radial distance of 96.1 AU, and Voyager 2 is at 77.0 AU. Because of a failure of the wideband receiver on Voyager 2, the ability to measure dust impacts on that spacecraft ended at a distance of about 64 AU. The impact rates also do not depend on ecliptic latitude or longitude, although the data coverage for these two parameters is much more limited than for heliocentric radial distance.

If we assume that the spacecraft is effectively sweeping up the particles, we can make a rough estimate of the number density of the impacting particles by using the formula n = R/UA, where R is the impact rate, A is the cross-sectional area of the spacecraft, and U is the heliocentric speed of the spacecraft. Using A = 1.66 m^2, which is our best estimate of the effective area of the spacecraft for detecting dust impacts, and U = 18 km s^{-1}, which is a typical spacecraft velocity, the average number density works out to be about 4 x 10^{-8} m^3. The mass of the impacting particles is more difficult to estimate, but is believed to be on the order of 10^{-10} to 10^{-11}g (i.e., in the micron size range), mainly because the impacts have waveforms very similar to those observed near Saturn's ring plane which are thought to be due to micron-sized particles. The absence of significant latitudinal or radial gradients suggests that the particles probably do not originate from planetary rings, moons, or asteroids. Most likely they are of interstellar origin, or possibly from objects orbiting the Sun at great distances, such as comets. Dust originating from Kuiper belt objects, which are confined relatively close to the ecliptic plane, can probably be ruled out because the impact rate does not show any dependence on distance above or below the ecliptic plane out to at least z = 50 AU. We have also looked for evidence of dust streams, such as might be related to comet trails, and none were found. The time interval between impacts has a good fit to a Poisson distribution, indicating a purely random distribution.

SCATTERING BY "BIRD'S-NEST" –TYPE MATERIAL AND LARGE DUST AGGREGATES: MICROWAVE ANALOGUE MEASUREMENTS. B. Å. S. Gustafson[1] and A. J. Espy[1], [1]Department of Astronomy, University of Florida, Gainesville, Florida 32611, USA.

Introduction: Planetesimals in the outer parts of the solar system, beyond the ice-line, are now known as comet nuclei and Kuiperbelt objects. These are believed by many to preserve solids that predate the solar system, solids that formerly were interstellar grains[1]. These grains brought the matter that the solar system is made of to the solar nebula and are our solar system's link to the stars that predates it. Evidence for how these grains grow into aggregates (ballistic or cluster-cluster, randomly oriented or aligned, with volatile solids preserved or evaporated, etc…) is possibly still preserved in the very morphology of comet nuclei and Kuiperbelt objects on the scale of tens to hundreds of micron. This structure may be exposed in dusty comet comae and dust tails as sunlight strikes grains shed by comet nuclei or it may be exposed as objects collide creating what has become known as dust bands in the Zodiacal cloud.

Objective: Our long-term objective is to extract statistically significant information on this structure from bodies across the Kuiperbelt, among comets and primitive type asteroids. A step along the way is the search for optical properties that differentiate between relevant particle morphologies and might be observable. Work on extraction of scattering properties by complex grains with morphologies similar to the "Bird's-Nest" structure[2] has long been part of theoretical and experimental efforts in our group at the University of Florida and by several other researchers. Earlier work has however been confined either to smaller grains, simpler structures, or both. This limitation to theoretical works is because the complexity of the scattering body and most severely affects large structures. Experimental works using optical light is limited by control over the experiment while the size of the analogue models used in experiments scaled to microwave frequencies usually is the limitation. This was a formal limitation in the famous microwave laboratories built by Greenberg et al. in New England respectively Giese et al. in Germany. This limitation was overcome in the present microwave laboratory at the University of Florida due primarily to the antenna design. However the challenge to build large models involving thousands or tens of thousands of individual particles was not previously overcome.

Results: We will present results for aggregates of spheres where each sphere represents a grain grown by condensation in the outflow from red giant stars or from supernovae. These oldest of solids are believed to be amorphous refractories with amorphous organic refractory mantles and therefore to grow at equal rates in all directions. This should lead to equidimensional growths of size in the 0.1 micron range that we represent by spheres. These can be homogeneous since the refractive index of both core and mantle is believed to be in the 1.7 to 1.8 range in real part and to have an imaginary part in the 0.01 range or less[3]. This means that although the chemical composition is different in the core and mantle, the optical properties of the core and mantle materials are the same to within the range of uncertainties and may thus be represented by a single analogue material that has the appropriate refractive index at the laboratory set of frequencies. We represent the classical size interstellar grains by sets of two or three spheres since they are known to be elongated with 2:1 to 3:1 aspect ratios. This property of grain elongation (and alignment) is evident from interstellar polarization, a linear polarization in extinction. Ices with inclusions of smaller grains are believed to form a second mantle on dust in the molecular clouds and the nebulae from which planetary systems form. These dirty ice mantles played an important role in determining the packing in grain aggregates that formed in the outer parts of the solar system where the ice mantles survive nebula heating from contraction. Analogue models of ice-less aggregates containing a few thousand spheres have been built by first joining spheres in sets of two or three and then by stacking these together in a manner that simulates ballistic aggregation taking the ice mantle into account. These have then been joined together to form successively larger models. This means that we simulate aggregates that once grow from grains that had ice mantles. The ice later sublimated as the material heated up causing the release of the dust aggregates and surely caused many aggregates to break into pieces. The ice sublimating away is believed to leave behind the low packing aggregates with approximately 90% void that we have simulated in our models. These are larger although in many ways similar to earlier "Bird's-Nest" models but we emphasize that since these are break-up products, they are not likely to retain the overall fractal dimension character that is so well established a characteristic of growing aggregates. The models we made are therefore of approximately equal packing throughout. Some aggregates however, have multiple centers with denser packing corresponding to the central parts of aggregates that formerly existed as separate aggre-

gates (Figure 1). The growth process we simulate has these formerly separate aggregates colliding and sticking together in a cluster-cluster aggregation process.

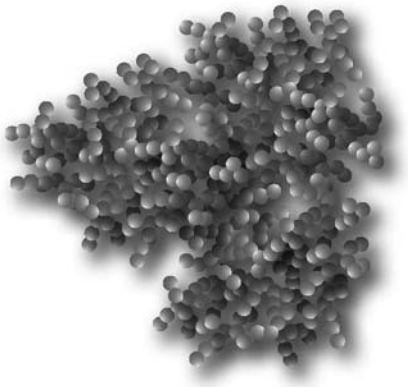

Figure 1) Sample aggregate based on irregular grain distribution and the packing of the refractory materials of 10% in an ensemble whose morphology or structure depends strongly on the scale and the corresponding growth regime

The aggregates are similar to the original "Bird-Nest" structures by Greenberg and Gustafson[2] in that they have approximately 10% packing (90% void). The major differences from the earlier model are in the size of the aggregates and the fact that there are multiple centers of higher packing density corresponding to aggregates grown in a ballistic process and then as cluster-cluster aggregation. The aggregates simulate parts of a large body (comet nucleus or Kuiper belt object) that has broken off and therefore has no low packing outer parts or protruding linear growths. The mass depends on the linear dimension cubed and therefore has a whole rather than fractal dimension. These aggregates are also not fractals since their structure is scale dependent. There are specific growth regimes that dominate depending on the scale. Condensation occurs on the 0.1 micron scale and below, ballistic aggregation on the scale of a few microns and cluster-cluster aggregation on larger scales.

We find that polarization, color and angular brightness distributions all depend on the specific packing but uniqueness is a more difficult issue. We discuss ways in which scattering properties might be used to recognize the specific structures we have modeled. Specifically we address how this might be used to recognize if the parent body generating the observed dust had differentiated by the time of the dust release. If the parent body is fund not to be differentiated, we like to know on what scale cluster-cluster aggregation took place.

Acknowledgements: The authors gratefully acknowledge Mr. Michael Pavel for his assistance in the laboratory. This work is supported by NASA through its Planetary Atmospheres Program.

References: 1) Grün, Gustafson, Dermott, and Fechtig, Eds., "Interplanetary Dust", Springer Verlag, pp. 509-567, (2001).
2) Greenberg, J.M., and B.Å.S. Gustafson, "A Comet Fragment Model for Zodiacal Light Particles", *Astron. Astrophys.*, **93,** pp. 35-42 (1981).
3) Gustafson B.Å.S., J.M. Greenberg, L. Kolokolova, R. Stognienko, and Y.-l. Xu. "Scattering Theory and Laboratory Simulations", in "Interplanetary Dust", (Grün, Gustafson, Dermott, and Fechtig, Eds.) Springer Verlag, pp. 509-567, (2001).

Ring Plane Crossings with the Cassini CDA Instrument: Saturation Analysis and Deadtime Correction.

S. Helfert[1] [1]Max-Planck-Institut für Kernphysik, Saupfercheckweg 1, 69117 Heidelberg, Germany. Stefan.Helfert@mpi-hd.mpg.de

CDA Instrument: The Cosmic Dust Analyzer[1] onboard Cassini comprises two distinct instruments: the Dust Analyzer (DA) and the High Rate Detector (HRD). The HRD is capable of counting thousands of impacts per second on its PVDF foils, whereas the DA instrument was designed to process about one impact event per second. The DA event processing consists of recording up to 2000 digital values for each of the 4 entrance channels and the Time-of-Flight mass spectrometer, computing key parameters, counting and classifying the event and filtering, compressing, and storing the raw data until delivery to the spacecraft Solid State Recorder.

Sensitivity: Early cruise measurements and the Jupiter Flyby already demonstrated that the sensitivity of the DA instrument exceeded the design criteria. The detection of Saturnian stream particles already at a distance of 1100 R_S was an additional result. Inside the saturnian system, during Ring Plane Crossings, the DA instrument is in saturation for prolonged periods of time. During these hour-long periods the DA is analyzing only a fraction of the incoming particles, so no count rates can be derived. Due to the high mass threshold of the HRD instrument, HRD cannot fill in the count rates for the dust environment that CDA is exposed to.

Instrument Dead Time Variation: One of the design criteria for the DA instrument was that the dead time between measurements should be within a one-second range and be independent of the processing complexity for the previous recorded event. To accomplish this, the dead time calculation was tied to a slow (8 Hz) periodic interrupt. Due to the discrete effects of this design, the variation of the dead time is of the order of 125 ms. To improve analysis of the DA count rates also during saturation phases, the dead time algorithm is upgraded in the current development Flight Software version. In this new version the DA dead time and the time between the opening of the measurement channels and the event trigger (live time) are measured and stored on a millisecond basis.

Laboratory Results: First ground test results from implementing this modification will be presented. A preliminary dead time correction for previous saturation phases will be demonstrated.

Enhancing Dead Time Correction: The lab tests and on-board data collected during saturation phases in Ring Plane Crossings in 2006 will be used for enhancement of the Dead Time correction for the rate[2]:

$$r_{corr} = \frac{r}{1 - r \cdot \tau}$$

Summary: Measuring, storing, and downlinking the instrument dead and live times in higher resolution should lead to accurate number density values even in periods of saturation.

References:

[1] Srama, R. et al.(2004) *Space Science Reviews 114, 465-518*, The Cassini Cosmic Dust Analyzer.

[2] Horanyi, M., Grün, E. (2005) private comm.

MODELLING ION BEHAVIOUR IN THE CASSINI COSMIC DUST ANALYSER. Jon K. Hillier[1], N. McBride[1] and S. F. Green[1].
[1]Planetary and Space Sciences Research Institute, The Open University, Milton Keynes, MK7 6AA, UK, j.k.hillier@open.ac.uk.

Interpreting the time of flight (TOF) mass spectra produced by the Cosmic Dust Analyser (CDA) on the Cassini spacecraft requires accurately identifying which ion species contribute to which spectral peaks. The relationship $t = a\sqrt{m}+b$ (t: time, a:stretch parameter relating to instrument field strengths, m:ion mass and b:zeropoint offset), usually used for calibrating TOF mass spectra is complicated in the CDA as the instrument does not perform any ion energy discrimination (such as that obtained by using a reflectron). The resulting spread in ion energies (and hence arrival times) tends to broaden and/or merge individual peaks, with plasma shielding, ion trajectory path length differences and field strength changes further affecting the spectra.

Hypervelocity dust impacts using a Van de Graaff generator to accelerate dust in the laboratory can be used to investigate the plasma (and spectra) produced by particles with a limited range of compositions, masses and velocities but this approach is unable to recreate the range of impact characteristics observed by CDA *in-situ*.

In this paper we present initial results from spectral modelling using the CDACAD numerical simulation software. This software uses the velocity verlet algorithm to simulate ion trajectories within the CDA instrument, allowing spectra to be created from impact plasmas of arbitrary composition with arbitrary initial velocity distributions. All of the CDA channels are simulated, at instrument-accurate sampling rates, allowing not only spectra to be recreated but also an estimation of ion losses to other parts of the instrument to be made. We present simulated fits to a variety of different types of flight spectra and comment on the implications for the impact plasma conditions.

SUBARU/COMICS OBSERVATIONS OF COMETARY DUST AND DUST AROUND YOUNG STARS

M. Honda[1] and COMICS team, [1]Institute for Space and Astronautical Science / JAXA (3-1-1 Yoshinodai, Sagamihara, Kanagawa, 229-8510, Japan; hondamt@ir.isas.jaxa.jp) .

Introduction: Crystalline silicate which is often found toward dust in Oort cloud comets (OCs) is supposed as a probe of thermal history of silicate dust. Since silicate dust in the interstellar matter (starting material) is completely amorphous [1], presence of crystalline silicate dust in OCs indicate that initially amorphous silicate dust must have experienced heating process which resulted in silicate dust crystallization. To understand when and how dust processing occurred at the early stage of solar-system / exo-planetary system formation, we investigated properties of dust around young stars (especially low-mass young stars which is similar to our Sun). Furthermore, to investigate how efficiently radial mixing have occured in the solar-nebula, we observed dust from Edgeworth-Kuiper Belt comets (EKBCs) which may be formed at more distant region than OCs.

Observations: We made mid-infrared low-resolution spectroscopic observations (R~250) of cometary dust and dust around young stars using the mid-infrared instruments COMICS [2,3] on 8.2m Subaru Telescope. We also made imaging observations at 8.8μm and 12.4μm to estimate absolute flux. Observations of standard stars for flux calibration and atmospheric absorption correction are also made before and/or after observation of the target.

Results: A 10μm silicate emission feature is frequently seen toward low-mass young stars and also toward EKBCs with signatures of not only amorphous silicate but also crystalline silicate. We derived fraction of crystalline silicate by fitting the model spectrum to the observed spectrum. Based on our analysis, we found following things. 1) Crystalline silicate dust around young stars seems to be formed at very early stage of star formation (~1 Myr or earlier). 2) Crystalline silicate is also found toward cometary dust from EKBCs, indicating that radial transportation of crystalline silicate dust toward outer solar nebula is very efficient.

References: [1] Kemper, F. et al. (2004) *ApJ, 609* , 826. [2] Kataza H. et al. (2000) *SPIE, 4008*, 1144. [3] Okamoto Y. J. et al. (2003) *SPIE, 4841*, 169.

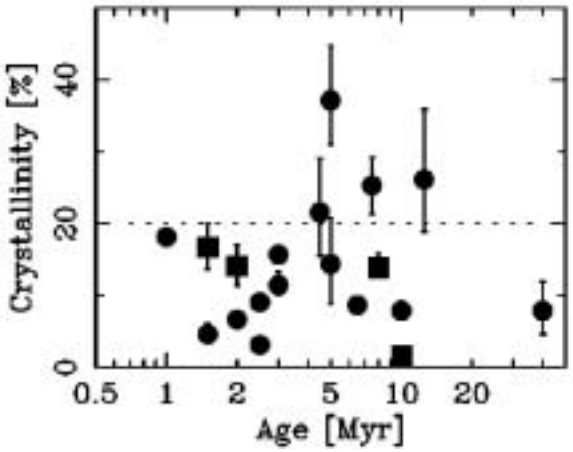

Figure 1: Fraction of crystalline silicate dust derived from model fitting to the silicate feature in 10 μm spectra of T Tauri stars against stellar age. Stellar age is estimated by comparison with theoretical evolutionary tracks in HR diagrams (Siess et al. 2000). Even at very young stage (~1 Myr) about ~20% of silicate dust appear in the form of crystalline silicate indicating that crystalline silicate formation occurs at the very early stage.

Dust Plasma Interactions in Planetary Rings

Mihály Horányi

Laboratory for Atmospheric and Space Physics, and Department of Physics, University of Colorado, Boulder, Colorado 80309-0392, USA

Planetary rings are our best examples of environments where dusty plasma effects can establish the size and spatial distributions of small grains. Simultaneously, dust often influences the composition, density and temperature of the plasma surrounding it. The dynamics of charged dust particles can be surprisingly complex and fundamentally different from the well understood limits of gravitationally dominated motions of neutral particles, or the adiabatic motion of electrons and ions in electromagnetic fields that dominate gravity [1].

This talk will focus on recent Cassini observations at Saturn that are best explained by theories describing the effects of the magnetospheric fields and plasmas on the rings. We will compare the theoretical model predictions with in situ and remote sensing observations of the E-ring. We also discuss the physics describing the formation of the `spokes' and their apparent lack to date in the Cassini images.

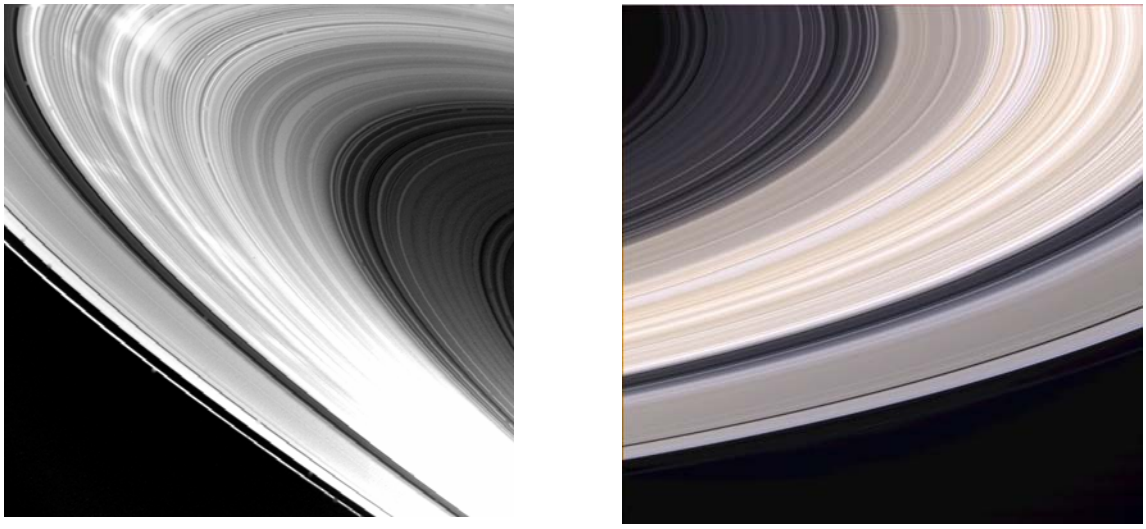

Fig.1 Images of Saturn's main rings taken by the Voyager (left) and Cassini (right) spacecraft. Voyager observed bright radial features that intermittently appeared above the rings. Cassini did not find these during its first year in orbit around Saturn.

[1] M. Horányi, T. W. Hartquist, O. Havnes, D. A. Mendis and G. E. Morfill, Dusty Plasma Effects in Saturn's Magnetosphere, Reviews of Geophysics, 42, RG4002, 2004

MIGRATION OF DUST PARTICLES TO THE TERRESTRIAL PLANETS. S. I. Ipatov, *University of Maryland, USA (siipatov@mail333.com)*, J. C. Mather, *NASA/GSFC, Greenbelt, MD, USA*.

Introduction: There are a lot of papers on migration of dust (see references in [1-2]). In contrast to papers by other scientists, we study the orbital evolution of dust particles for a wider range of masses of asteroidal and cometary particles and consider also migration of dust particles produced by comets 10P and 39P.

Model: We integrated [1-2] the orbital evolution of about 12,000 asteroidal, cometary, and trans-Neptunian dust particles under the gravitational influence of planets, the Poynting-Robertson drag, radiation pressure, and solar wind drag, varying the values of the ratio β between the radiation pressure force and the gravitational force from $\leq$0.0004 to 0.4 (for silicates, such values correspond to particle diameters between $\geq$1000 and 1 microns). The considered cometary particles started from comets 2P, 10P, and 39P. A few hundred of particles were considered in each run. In our runs orbital elements were stored with a step of d_t of $\leq$20 yr for asteroidal and cometary particles and 100 yr for trans-Neptunian particles. The planets were assumed to be material points; however, using orbital elements obtained with a step d_t, we calculated the mean collision probability of a particle with the planet during the particle lifetime P=P_Σ/N, where P_Σ is the probability for all N considered particles. The relative error per integration step less than 10^{-8} was adopted. The integration continued until all of the particles either collided with the Sun or reached 2000 AU from the Sun.

Collision probabilities of dust particles with planets: The probability P of a collision of an asteroidal dust particle with the Earth was found [2] to have a maximum ($\sim$0.001-0.02) at 0.002$\leq\beta\leq$0.01, i.e., at diameters of particles $d\sim$100 μm. This is in accordance with cratering records in the lunar soil and also with particles record on the panels of the Long Duration Exposure Facility, which showed that the mass distribution of dust particles encountering Earth peaks at d=200 μm. At β>0.01 collision probabilities of asteroidal particles with the terrestrial planets decreased with growing β. For Venus these probabilities didn't differ much from those for Earth, whereas for Mars they were by an order of magnitude smaller at $\beta\geq$0.01 compared to Earth, and nearly similar to those for Earth at $\beta\sim$0.0004-0.001.

Collision probability P of a particle started from Comet 10P with a terrestrial planet sometimes differed by a factor of several from that for an asteroidal particle of the same size. In turn, for Comet 2P dust debris, the P values were found usually smaller than for asteroidal and 10P particles: for Earth at 0.002$\leq\beta\leq$0.01, P was by an order of magnitude smaller for 2P particles than for asteroid particles. For 2P particles at some β, P is by a factor of 2 or 4 greater for Venus than for Earth.

For trans-Neptunian and 39P particles, maximum values of the probability of collisions with the Sun (0.2-0.3) were reached at 0.05$\leq\beta\leq$0.1. For $\beta\geq$0.05, the fraction of trans-Neptunian particles collided with the Sun was less than that of asteroidal particles by a factor of 4-6.

Probabilities of collisions of trans-Neptunian particles with Earth and Venus at 0.01$\leq\beta\leq$0.2 were $\sim(0.3-4)\cdot10^{-4}$ and were usually less than those for asteroidal particles by a factor of less than 4. The ratio of values of time T during which a particle has perihelion less than 1 AU for asteroidal particles to the values of T for trans-Neptunian particles was about 3-7 at $\beta\geq$0.1 and about 20 at β=0.05. The mean values e_m and i_m of eccentricities and inclinations at distance R=1 AU from the Sun were mainly greater for trans-Neptunian particles than those for asteroidal particles. Nevertheless, the ratio P/T was greater for trans-Neptunian particles. It may be caused by that perihelia or aphelia of migrating trans-Neptunian particles more often were close to the orbit of the Earth, or the fraction of Earth-crossing trans-Neptunian particles with small e and i was greater (though e_m and i_m were greater) than for asteroidal particles.

Probabilities P_E of collisions of trans-Neptunian and 39P dust particles with the Earth were usually smaller by a factor of several or more than those for asteroidal and 10P particles of the same size. At β=0.0001 one 39P particle moved in an Earth-crossing orbit located inside Jupiter's orbit for 6 millions of years, and the values of P and T for this run were much greater than those for other 39P runs. For 39P particles greater than 1000 μm, one need to consider many thousands of particles in order to get reliable statistics because for such runs the probability of a collision of one particle with the terrestrial planets can be greater than the total probability of collisions of thousands other particles. Comet 39P is located outside Jupiter's orbit ($a\approx$7 AU), and studies of the orbital evolution of dust particles produced by this comet help to better understand migration of trans-Neptunian particles to the terrestrial planets at small β. At 0.01$\leq\beta\leq$0.2 the values of P_E for trans-Neptunian dust particles were similar to those for 39P particles ($\sim10^{-4}$), but the times in Earth-crossing orbits for trans-Neptunian particles were smaller by a factor of several than those for 39P particles. Due to

a small fraction of large (>1000 μm) particles that can move in Earth-crossing orbits for a long time, it may be possible that the probability of a collision of such trans-Neptunian particle with the Earth can be of the same order of magnitude as that for d<50 μm, but much more runs are needed for accurate estimates.

Interstellar particles can be effective in destruction of trans-Neptunian dust particles through collisions, especially with grains between 9 μm and 50 μm, as it is argued in [3]. Larger particles may survive because interstellar grains are too small to destroy them in a single impact. Since the total mass of the trans-Neptunian belt exceeds that of the asteroid belt by more than two orders of magnitude, and the derived in our model mean residence times ratio in orbits with perihelion distance q<1 AU for asteroid and trans-Neptunian particles is less than 20 at $\beta\geq$0.05, then for $d\sim$1-10 μm the fraction of trans-Neptunian dust of the overall dust population can be significant even at R<3 AU.

Distribution of migrating dust particles: Based on our runs, we studied [2] the distribution of spatial density n_s (i.e., the number of particles per unit of volume) near ecliptic over distance R from the Sun. For asteroidal particles, n_s quickly decreases with an increase of R. So asteroidal dust particles cannot explain the constant spatial density of dust particles at $R\sim$3-18 AU. At such distances, many of the dust particles could have come from the trans-Neptunian belt and from comets. In our runs at $\beta\geq$0.05, spatial density n_s of trans-Neptunian particles near ecliptic at R=1 AU was greater than at R>1 AU. At 0.1$\leq\beta\leq$0.4 and 2<R<45 AU (at β=0.05 for 11<R<50 AU) for trans-Neptunian particles, n_s varied with R by less than a factor of 4, but at R=5 AU it was smaller by at least a factor of 2 than at 15 AU.

Velocities of dust particles: Ipatov et al. [4-5] studied how the solar spectrum is changed by scattering by dust particles. Positions of particles were taken from the runs of migration of dust particles. For each such stored position, we calculated many ($\sim10^2$-10^4 depending on a run) different positions of a particle and the Earth during the period P_{rev} of revolution of the particle around the Sun, considering that orbital elements do not vary during P_{rev}. Three different scattering functions were considered [2]. For each considered position, we calculated velocities of a dust particle relative to the Sun and the Earth and used these velocities and the scattering function for construction of the solar spectrum received at the Earth after been scattering by different particles located at some beam (line of sight) from the Earth. The direction of the beam is characterized by elongation ϵ and inclination i. Particles in the cone of 2° around this direction were considered. In each run, particles of the same size (at the same β) and the same source (i.e., asteroidal) were studied. Ipatov et al. [5] and Madsen et al. [6] compared the rotation curves, i.e., plots of velocities of Mg I line (at zero inclination) versus elongations ε (measured eastward from the Sun), with the observational plots obtained by Reynolds et al. [7]. The rotation curves obtained for different considered scattering functions were similar for 30°<ε<330°, the difference was greater for more close direction to the Sun. The difference between different plots for different sources of dust was maximum at ε between 90° and 120°. In our opinion, the main conclusion of the comparison of such curves is that asteroidal dust doesn't dominate in the zodiacal light and a lot of zodiacal dust particles were produced by high eccentricity comets (such as comet 2P Encke). Significant contribution of cometary dust was considered by several other authors. For example, based on cratering rates from an ensemble of Earth- and Lunar-orbiting satellites, Zook [8] estimated that the cometary contribution to the near-Earth flux of particles is ∼75%.

Conclusions: Probabilities of collisions of migrating asteroidal and cometary dust particles with the terrestrial planets during the lifetimes of these particles were maximum at diameter $d\sim$100 μm, which is in accordance with the analysis of microcraters.

Cometary dust particles (produced both inside and outside Jupiter's orbit) are needed to explain the constant spatial density of dust particles at 3-18 AU. The spatial density of migrating trans-Neptunian particles near Jupiter's orbit is smaller by a factor of several than that beyond Saturn's orbit. Only a small fraction of asteroidal particles can get outside Jupiter's orbit.

Comparison of velocities of particles obtained in our runs with the results of observations also show that only asteroidal dust particles cannot explain these observations, and particles produced by high-eccentricity comets (such as Comet Encke) are needed for such explanation.

Several our recent papers are presented on astro-ph.

References: [1] Ipatov S. I., Mather J. C., and Taylor P. (2004) *Annals of the New York Acad. of Sciences, 1017*, 66-80. [2] Ipatov S. I. and Mather J. C. (2005) *Advances in Space Research*, in press. [3] Liou J.-C., Zook H. A., Dermott S. F. (1996) *Icarus, 124*, 429-440. [4] Ipatov S. I. et al. (2005) *LPSC XXXV*, abstract #1266. [5] Ipatov S. I. et al. (2005) *BAAS*, late abstracts of AAS 206 Meeting, #449, in press. [6] Madsen G. J. et al. (2005) *this abstract book*. [7] Reynolds R. J., Madsen G. J., Moseley S. H. (2004) *Astrophys. J., 612*, 1206-1213. [8] Zook H. A. (2001) in: Peucker-Ehrenbrink, B. and Schmitz, B. (Eds.) *Accretion of extraterrestrial matter throughout Earth's history*, Kluwer, New York, 75-92.

SYNCHROTRON X-RAY FLUORESCENCE ANALYSIS OF DUST PARTICLES. H. A. Ishii[1], K. Luening[2], S. Brennan[2], P. Pianetta[2], G. Matrajt[3] and J. P. Bradley[1], [1]Institute for Geophysics and Planetary Physics, Lawrence Livermore National Laboratory, Livermore, CA 94550, USA (hope.ishii@llnl.gov), [2]Stanford Synchrotron Radiation Laboratory, Stanford Linear Accelerator Center, Stanford, CA 94025, USA (brennan@stanford.edu), [3]Department of Astronomy, University of Washington, Seattle, WA 98195.

Introduction: Synchrotron x-ray fluorescence (SXRF) studies carried out on a microprobe endstation allow non-destructive analysis of both major and trace element abundances in particles only microns in size. The technique has been applied to IDPs captured in the stratosphere to study atmospheric entry effects such as stratospheric contamination and frictional heating [1, 2]. SXRF will also be applied to the analysis of samples from NASA's Stardust mission [3] returning to Earth in January of 2006 with cometary dust particles captured in silica aerogel collectors during its flyby of the comet Wild-2. For Stardust particles, as for IDPs, trace element analysis of volatiles may provide an indication of the degree of thermal processing during capture in the aerogel collectors. Assuming negligible processing, trace elements can be used to study petrogenetic relationships between Stardust particles and other known extraterrestrial materials. In general, analysis of trace element abundances in extraterrestrial materials is highly relevant because variations in concentration patterns of these elements may act as signatures for origin and conditions of formation of the carrier mineral phases [4].

A number of challenges must be overcome for trace element studies by SXRF: sample preparation, contamination, choice of sample mount, potential for sample damage in the x-ray beam and positional stability of the beam on the sample. IDP SXRF studies to date offer only limited discussion of experimental setup and analytical limitations. We discuss here the experimental requirements for obtaining high quality SXRF data on small particles for trace element analysis and our progress in achieving this goal.

Experimental Methods: We collected SXRF data from several chondritic porous IDPs on a scanning fluorescence microprobe endstation currently being commissioned on Beamline 6-2 at the Stanford Synchrotron Radiation Laboratory (SSRL). The final focus is provided by a Kirkpatrick-Baez mirror pair capable of focusing monochromatic x-rays into a micron-sized spot. The current non-optimized photon flux for a ~3 μm spot is ~$5x10^8$ photons/s, and the x-ray energy range extends past the Br K absorption edge. We have previously demonstrated SXRF mapping of major elements at low and high spatial resolutions [5]. For this early trace element work during endstation commissioning, there was unusual beam motion at the source, and we used a ~10 μm spot size to encompass entire IDP particles and sections. In future work, we will combine trace element mapping with TEM imaging and EDS analysis as discussed below.

Experimental Requirements and Results: To obtain the best quality SXRF data on small particles, we want no sample damage and high sample stability with no extraneous fluorescence to obscure peaks of interest and reduce signal-to-noise ratios.

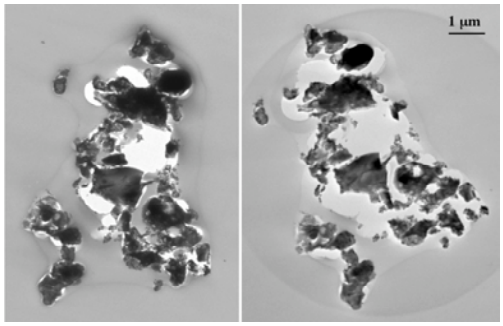

Fig. 1: Evidence of ozone damage without a He environment: Bright field TEM images of a 200 nm section of IDP W7154I1 before (left) and after (right) 7 hours of x-ray irradiation.

Damage to the sample by x-rays. In an initial estimation of particle heating in the beam, a microthermocouple (35 micron welded bead) showed a rise of only 0.5°C before stabilizing in temperature in the x-ray beam. In addition, a 200 nm thick TEM section of a chondritic porous IDP was scanned in the x-ray beam for 7 hours with a 3 μm spot. TEM analysis before and after x-ray irradiation showed no evidence of structural or chemical changes due to heating in the x-ray beam. (Sample heating will be reevaluated with the final optimized photon flux.) There is clear evidence of attack by ozone formed by x-rays interacting with air. Ozone etches the sample, especially organics like the embedding epoxy, particularly near voids (Figure 1). We subsequently employed a He "shower", a gentle flow of He over the sample and most of the beam path to the detector to eliminate ozone damage by excluding air. This has the important advantage of greatly reducing the Ar fluorescence and improving detection of low Z elements such as Na, Al and Mg.

Sample mounting. Mounting is a critical challenge for particle sizes on the order of 10 μm. We require excellent positional stability since sample motion, due to mechanical or thermal instability, results in the x-ray beam wandering on the sample or off the sample completely. We collected spectra from two forms of samples: thin sections and whole IDPs.

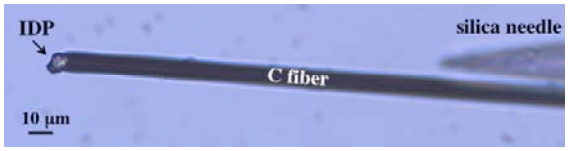

Fig. 2: An IDP (L2005AN6) mounted atop a C fiber attached to a silica needle (tip visible in background).

For bulk analysis of whole, intact IDPs, a 10 μm diameter C fiber was glued to the end of a 1 mm diameter silica needle leaving 100-200 μm of fiber extending from the end of the needle. Each IDP was mounted by micromanipulator on the end of the C fiber with a tiny amount of partially-cured embedding epoxy (Figure 2). These mounts proved highly stable and presented the particle to the x-rays free of any substrate. For whole IDPs, 13.5 keV incident x-rays accessed trace elements up to Br. Figure 3 shows the SXRF spectrum (unprocessed) of a mounted IDP.

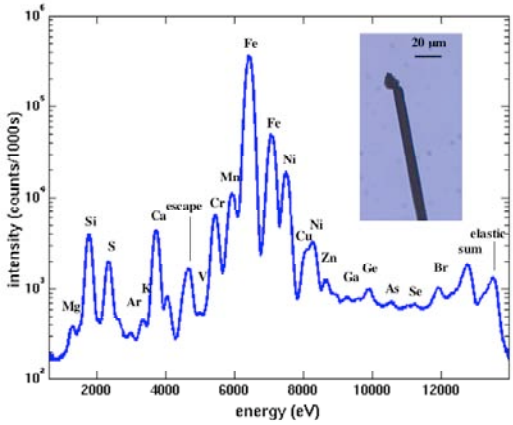

Fig. 3: SXRF spectrum from a whole chondritic porous IDP L2005AN5 mounted on a C fiber.

Microtomed particle thin sections allow correlation of SXRF and TEM data. In this way, local trace element abundances in particles can be correlated with local mineralogy to gain insight into particle origins and processing. IDP sections were precision-centered in 400 μm aperture Cu TEM grids on C/Formvar substrates using a method developed in the cosmic dust lab at U. of Washington (Brownlee). To avoid exciting fluorescence from the grid, spectra from thin sections were collected ~200 eV below the Cu K edge at 8780 eV. Due to overlap of the Cu Kα resonant Raman scattering peak (~940 eV below the incident energy) with Fe or Ni, Cu is a poor grid material even at energies below the Cu K edge. To access higher-Z trace elements in thin sections, future studies will be carried out using low-Z (C, Be) grids. Figure 4 shows a microtomed thin section in a Cu TEM aperture grid and its SXRF spectrum (collected in He). Knowledge of trace element contaminants in mounting media is critical. The Na and Cl peaks in Figure 4, for example, are likely due to salt in the epoxy, and the Cu shoulder on the Ni peak in Figure 3 is not associated with the particle.

We have made much progress in attaining high quality SXRF spectra from small particles. Sample damage in the beam is being assessed and addressed. C fiber mounts are well-suited to whole IDP studies, and appropriate TEM grids have been identified for thin section studies. Spectra obtained show excellent signal-to-noise, and we are in the process of analyzing them for quantitative results.

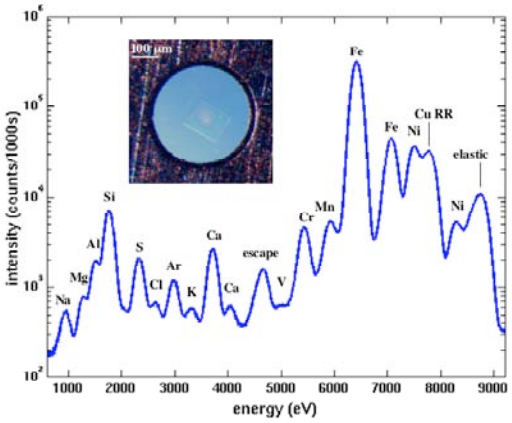

Fig. 4: SXRF spectrum from a microtomed thin section of IDP W7154I1, 200 nm thick, mounted in a TEM aperture grid. Epoxy discoloration in the inset optical image is due to prior TEM analysis rather than x-ray exposure.

References: [1] Flynn G. J. et al. (1996) *LPS XXVII*, 367-368. [2] Kehm K. et al. (2002) *MAPS, 37*, 1323. [3] Brownlee, D. E. et al. (2003) *JGR, 108*, SRD 1-15. [4] Kashiv, Y. et al. (2001) *LPS XXXII*, Abstract #2192. [5] Ishii, H. A. et al. (2005) *LPS XXXVI*, Abstract #1393.

Acknowledgements: This work was performed in part under the auspices of the U.S. Department of Energy, NNSA by the Lawrence Livermore National Laboratory under contract No. W-7405-Eng-48 and in part at the Stanford Synchrotron Radiation Laboratory, a national user facility operated by Stanford University on behalf of the U.S. Department of Energy, Office of Basic Energy Sciences. This work was performed as part of the Bay Area Particle Analysis Consortium (BayPAC) and was supported by NASA Grant NNH04AB49I. We thank Z. Dai for valuable assistance with TEM.